DNA-TR-86-401

ANALYSIS OF THE BURNING REGION AND PLUME OF A LARGE FIRE

R. D. Small, et al.
Pacific-Sierra Research Corporation
12340 Santa Monica Boulevard
Los Angeles, CA 90025-2587

30 September 1986

Technical Report

CONTRACT No. DNA 001-85-C-0056

THIS WORK WAS SPONSORED BY THE DEFENSE NUCLEAR AGENCY
UNDER RDT&E RMC CODE B3460857642 RX RF 00003 25904D.

Prepared for
Director
DEFENSE NUCLEAR AGENCY
Washington, DC 20305-1000

Destroy this report when it is no longer needed. Do not return to sender.

PLEASE NOTIFY THE DEFENSE NUCLEAR AGENCY ATTN: TITL, WASHINGTON, DC 20305-1000, IF YOUR ADDRESS IS INCORRECT, IF YOU WISH IT DELETED FROM THE DISTRIBUTION LIST, OR IF THE ADDRESSEE IS NO LONGER EMPLOYED BY YOUR ORGANIZATION

DISTRIBUTION LIST UPDATE

This mailer is provided to enable DNA to maintain current distribution lists for reports. We would appreciate your providing the requested information.

☐ Add the individual listed to your distribution list.

☐ Delete the cited organization/individual.

☐ Change of address.

NAME: _____

ORGANIZATION: _____

OLD ADDRESS	CURRENT ADDRESS
_____	_____
_____	_____
_____	_____

TELEPHONE NUMBER: (___) _____

SUBJECT AREA(s) OF INTEREST:

_____	_____
_____	_____
_____	_____

DNA OR OTHER GOVERNMENT CONTRACT NUMBER: _____ _____

CERTIFICATION OF NEED-TO-KNOW BY GOVERNMENT SPONSOR (if other than DNA):

SPONSORING ORGANIZATION: _____

CONTRACTING OFFICER OR REPRESENTATIVE: _____

SIGNATURE: _____

CUT HERE AND RETURN

Director
Defense Nuclear Agency
ATTN: [redacted] TITL
Washington, DC 20305-1000

Director
Defense Nuclear Agency
ATTN: [redacted] TITL
Washington, DC 20305-1000

UNCLASSIFIED

SECURITY CLASSIFICATION OF THIS PAGE

AD-A186253

REPORT DOCUMENTATION PAGE

1a. REPORT SECURITY CLASSIFICATION UNCLASSIFIED	1b. RESTRICTIVE MARKINGS
2a. SECURITY CLASSIFICATION AUTHORITY N/A since Unclassified	3. DISTRIBUTION/AVAILABILITY OF REPORT Approved for public release; distribution is unlimited.
2b. DECLASSIFICATION/DOWNGRADING SCHEDULE N/A since Unclassified	
4. PERFORMING ORGANIZATION REPORT NUMBER(S) PSR Report 1672	5. MONITORING ORGANIZATION REPORT NUMBER(S) DNA-TR-86-401
6a. NAME OF PERFORMING ORGANIZATION Pacific-Sierra Research Corporation 6b. OFFICE SYMBOL (If applicable)	7a. NAME OF MONITORING ORGANIZATION Director Defense Nuclear Agency
6c. ADDRESS (City, State, and ZIP Code) 12340 Santa Monica Boulevard Los Angeles, CA 90025-2587	7b. ADDRESS (City, State, and ZIP Code) Washington, DC 20305-1000
8a. NAME OF FUNDING/SPONSORING ORGANIZATION 8b. OFFICE SYMBOL (If applicable) TDRP/Auton	9. PROCUREMENT INSTRUMENT IDENTIFICATION NUMBER DNA 001-85-C-0056
8c. ADDRESS (City, State, and ZIP Code)	10. SOURCE OF FUNDING NUMBERS PROGRAM ELEMENT NO. 62715H; PROJECT NO. RX; TASK NO. RF; WORK UNIT ACCESSION NO. DH008096

11. TITLE (Include Security Classification)
ANALYSIS OF THE BURNING REGION AND PLUME OF A LARGE FIRE

12. PERSONAL AUTHOR(S)
Small, R. D.; Larson, D. A.; Remetch, D.; and Brode, H. L.

13a. TYPE OF REPORT	13b. TIME COVERED	14. DATE OF REPORT (Year, Month, Day)	15. PAGE COUNT
Technical	FROM 841126 TO 860226	860930	68

16. SUPPLEMENTARY NOTATION
This work was sponsored by the Defense Nuclear Agency under RDT&E RMC Code B3460857642 RX RF 00003 25904D.

17 COSATI CODES			18. SUBJECT TERMS (Continue on reverse if necessary and identify by block number)
FIELD	GROUP	SUB-GROUP	
13	12		Nuclear Weapon Fires; Flambeau; Fire Winds; Fire Region Analysis; Area Fires; Atmospheric Response to Fire Plumes
04	02		

19. ABSTRACT (Continue on reverse if necessary and identify by block number)

The strongly buoyant flow generated in and around a large area fire is analyzed. Jump conditions applicable at the fire periphery are used to affect model problem closure, thus permitting calculation of induced fire winds independent of a far-field analysis. Combustion processes are modeled by a volume heat addition. The induced flow is compressible, with arbitrary changes in temperature and density allowed. In one parameter limit, a closed-form solution is developed that concisely describes the basic interchanges of energy and momentum as well as the role of pressure gradients in fire-wind generation. The full analysis is applied in simulation of the hydrothermodynamics of a multiple-fuel-bed Flambeau fire. Computed results duplicate observed flow patterns. A parametric analysis explores the influence of combustion zone dimensions, heating rate, radiation, and turbulent diffusion on the solution for even larger fires.

20. DISTRIBUTION/AVAILABILITY OF ABSTRACT ☐ UNCLASSIFIED/UNLIMITED ☒ SAME AS RPT. ☐ DTIC USERS	21. ABSTRACT SECURITY CLASSIFICATION UNCLASSIFIED
22a. NAME OF RESPONSIBLE INDIVIDUAL Sandra E. Young	22b. TELEPHONE (Include Area Code) (202) 325-7042 22c. OFFICE SYMBOL DNA/CSTI

DD FORM 1473, 84 MAR — 83 APR edition may be used until exhausted. All other editions are obsolete.

SECURITY CLASSIFICATION OF THIS PAGE
UNCLASSIFIED

19. ABSTRACT (continued)

Next, hydrocode solutions are presented for fires of city size with radii of several kilometers and flame heights of 100 m. The atmospheric response as a function of time is illustrated. Vortex motions generated by the fire influence both the inflow and plume structure. A fairly persistent circulatory flow develops below the tropopause. Periodically, however, the tropopause is penetrated, and an upper level counterrotating flow develops that may contain some combustion products from the central fire region. The results suggest the formation of distinct smoke strata in the lower atmosphere, with some particulate and aerosol mass entering the stratosphere. Keywords: Nuclear weapons fires; Earth atmospheric response to fire plumes.

SUMMARY

This report, presented in three sections, is based on two PSR studies of large area fires. Each study has been submitted at a specialist conference and has been published in the open literature. Our approach is to analyze separately the fire region and the atmospheric response to a large area fire. This is analytically convenient because the length scales vary widely. In a burning city, the flame height or height of the heat addition region is of order 100 m. On this scale, heat produces buoyancy and pressure gradients that induce fire winds and drive the free convection plume. The atmosphere responds to the convection flux on scales of order 10^3 m. The pressure and buoyancy forces are of lower order. Atmospheric gradients control the plume rise and spreading.

Section 1 is derived from a paper presented at the 26th Israel Annual Conference on Aviation and Astronautics, February 1984, and completes our development of an analytical model of the burning region of a large area fire. The formulation of boundary value problems for the fire region is discussed. The reduction of the full elliptic set to a parabolic system is described. A sample closed-form solution for weakly heated flows is presented. The results are used to describe the interactions between heat release, buoyancy production, generation of pressure gradients and induction of fire winds.

Section 2 is based on a presentation given at the Defense Nuclear Agency Conference on Large-Scale Fire Phenomenology, Gaithersburg, Maryland, September 1984. In it, we consider atmospheric response to a large area fire. This study complements the first, providing a highly resolved description of the plume motions. A simulation of an experimental Flambeau fire is used to establish confidence in the hydrocode capability. Results of the simulation clearly depict the merging of fire plumes from each fuel pile and the influence of crosswind on plume rise. Results of the simulation show relatively good agreement with the experimental observations.

Simulations of a 10-km radius area fire are also presented in Sec. 2. The development of a flow field that starts as a local flow to one that creates a large atmospheric disturbance is described. Although transient, a fairly persistent circulatory flow develops below the tropopause. Periodically, however, the tropopause is penetrated, and an upper-level counterrotating flow develops, which may contain some combustion products from the central fire region. The results suggest the formation of distinct smoke strata.

Section 3 is the list of references used in compiling both papers.

CONVERSION TABLE

Conversion factors for U.S. Customary to metric (SI) units of measurement

MULTIPLY → TO GET	BY	TO GET ← DIVIDE
angstrom	1.000 000 X E -10	meters (m)
atmosphere (normal)	1.013 25 X E +2	kilo pascal (kPa)
bar	1.000 000 X E +2	kilo pascal (kPa)
barn	1.000 000 X E -28	meter^2 (m^2)
British thermal unit (thermochemical)	1.054 350 X E +3	joule (J)
calorie (thermochemical)	4.184 000	joule (J)
cal (thermochemical)/cm^2	4.184 000 X E -2	mega joule/m^2 (MJ/m^2)
curie	3.700 000 X E +1	*giga becquerel (GBq)
degree (angle)	1.745 329 X E -2	radian (rad)
degree Fahrenheit	t_K = (t° f + 459.67)/1.8	degree kelvin (K)
electron volt	1.602 19 X E -19	joule (J)
erg	1.000 000 X E -7	joule (J)
erg/second	1.000 000 X E -7	watt (W)
foot	3.048 000 X E -1	meter (m)
foot-pound-force	1.355 818	joule (J)
gallon (U.S. liquid)	3.785 412 X E -3	meter^3 (m^3)
inch	2.540 000 X E -2	meter (m)
jerk	1.000 000 X E +9	joule (J)
joule/kilogram (J/kg) (radiation dose absorbed)	1.000 000	Gray (Gy)
kilotons	4.183	terajoules
kip (1000 lbf)	4.448 222 X E +3	newton (N)
kip/inch^2 (ksi)	6.894 757 X E +3	kilo pascal (kPa)
ktap	1.000 000 X E +2	newton-second/m^2 ($N-s/m^2$)
micron	1 000 000 X E -6	meter (m)
mil	2.540 000 X E -5	meter (m)
mile (international)	1.609 344 X E +3	meter (m)
ounce	2.834 952 X E -2	kilogram (kg)
pound-force (lbs avoirdupois)	4.448 222	newton (N)
pound-force inch	1.129 848 X E -1	newton-meter (N·m)
pound-force/inch	1.751 268 X E +2	newton/meter (N/m)
pound-force/foot^2	4.788 026 X E -2	kilo pascal (kPa)
pound-force/inch^2 (psi)	6.894 757	kilo pascal (kPa)
pound-mass (lbm avoirdupois)	4.535 924 X E -1	kilogram (kg)
pound-mass-foot^2 (moment of inertia)	4.214 011 X E -2	kilogram-meter^2 ($kg \cdot m^2$)
pound-mass/foot^3	1.601 846 X E +1	kilogram/meter^3 (kg/m^3)
rad (radiation dose absorbed)	1.000 000 X E -2	**Gray (Gy)
roentgen	2.579 760 X E -4	coulomb/kilogram (C/kg)
shake	1.000 000 X E -8	second (s)
slug	1.459 390 X E +1	kilogram (kg)
torr (mm Hg, 0° C)	1.333 22 X E -1	kilo pascal (kPa)

*The becquerel (Bq) is the SI unit of radioactivity; 1 Bq = 1 event/s.
**The Gray (Gy) is the SI unit of absorbed radiation.

TABLE OF CONTENTS

LIST OF ILLUSTRATIONS

LIST OF ILLUSTRATIONS (Concluded)

SECTION 1

VELOCITY FIELDS GENERATED BY LARGE FIRES

Most previous analyses of free-burning fires have focused on the physics of a buoyant plume.* The theories are restricted to small fires and are applicable only well above the flaming region. This section considers a large burning area and analyzes the strong interaction region in and around the fire. The formulation allows explicit calculation of the induced fire winds.

The buoyant plume above a small, free-burning fire is well described by integral theories that relate a sustained vertical flow to a weakly compressible gas state [Morton, Taylor, and Turner, 1956]. Dynamic pressure forces are assumed to be negligible, and a weak entrainment of ambient air is postulated at an effective plume edge. In and around the burning zone, however, such theories have limited applicability. The combustion processes foster large changes in temperature and density, creating a region of strong buoyancy and hence finite pressure gradients.

Entrainment criteria fail to accurately describe the flow field at and just above the fire periphery [Cox and Chitty, 1980]. The radial velocity decays inversely with height above the ground, and approaches a variation proportional to the center-line vertical velocity only well above the fire. It is the buoyancy-generated pressure forces, and not diffusive entrainment, that control the low-level induction of ambient air into the fire. The relationship between dynamic pressure and induced fire winds is indicated in the calculations of Smith, Morton, and Leslie [1975], though they assume small density changes (Boussinesq approximation) and do not seek fine resolution near the fire.

A model of the strongly buoyant flow generated in and around a large area fire is developed in the "Analysis" section, p. 3. A more highly resolved description of the mechanics of fire-wind generation

*Few studies attempt to model all regions simultaneously [Markatos and Pericleous, 1984].

results. A "large area fire" is defined here as one of large aspect ratio (fire width/maximum flame height). The analysis is thus applicable to fires ranging in size from the multiple-fuel-bed Flambeau experiments [Countryman, 1969] to arbitrarily larger fires [Larson and Small, 1982].

Attention is focused on the hydrothermodynamic processes in and around the combustion zone, and an uncoupled boundary-value problem describing the nonlinear relationships between heat release, strong buoyancy, and pressure gradients is developed. The induced fire winds are related to the characteristics of the combustion zone through jump conditions applicable at the fire periphery. The specification of local boundary conditions enables prediction of the fire winds without extensive numerical computations involving regions far from the combustion zone (see Smith, Morton, and Leslie [1975]). Thus a much more detailed view of the burning-zone physics is possible.

In one parameter limit, the model equations can be solved in closed form. The resulting solution concisely describes the basic interchanges of energy and momentum as well as the role of pressure gradients in fire-wind generation. Volume heating due to the combustion processes raises the temperature, lowers the density, and creates buoyancy. The pressure in and around the fire zone is then hydrostatically lowered, inducing the fire winds. That inflow is kinematically turned upward, forming the initial part of the convection column (plume).

A simulation of the near-fire velocity and thermodynamic fields induced by a Flambeau fire is presented under "Results," p. 17. Computed results are consistent with field observations and measurements. For larger fires, the dependence of temperature and fire winds on burning-zone dimensions, heating rate, turbulent mixing, and radiation is explored. Previous estimates based on plume theory [Lommasson, et al., 1968] suggest that fire-wind velocities vary as the cube root of the heating rate. The present analysis shows that velocities scale with the first power of the heating rate and the fire-zone aspect ratio. The stronger dependence on fire intensity is consistent with reported measurements [Adams, Williams, and Tregellas-Williams, 1972].

ANALYSIS.

The basic features and geometry of a large area fire system are illustrated in Fig. 1. The fuel bed may be either continuous or composed of discrete packets. However, it is sufficiently large that turbulence breaks the flame envelope, tending to keep flame heights uniform [Thomas, 1963]. Ambient air is drawn into the fire by a combination of physical processes involving heat addition, buoyancy, and pressure gradients. Air is heated in the combustion zone and rises buoyantly, carrying the products of combustion, to form a convection column. As cooler air replaces the rising, heated air, a high-speed inflow is produced in a surface layer that includes the lowest part of the convection column as well as the entire combustion zone. The portion of that layer which extends the depth of the combustion zone is here called the turning region. The present analysis examines the hydrothermodynamics of that region.

The turning-region flow is taken to be quasi-steady and axisymmetric. In Fig. 1, R represents the fire radius, H the maximum flame height, ΔR the difference between the maximum and minimum radii attained by the convection column in the turning region, and H_c a scale height for the column. For large area fires, $H < R$, and a characteristic combustion-zone aspect ratio is defined by

$$\varepsilon^{-1} = R/H , \quad \varepsilon << 1 . \tag{1}$$

Above the fire zone, the column radius decreases with height up to the "pinch point." That decrease is associated with the strong fire-wind convection, and thus the pinch-point altitude provides a reasonable measure of the turning-region height. For large experimental fires, that altitude is approximately five to ten flame heights above the fire [U.S. Forest Service, 1967], and the column radius is comparable to the fire radius. The pinch-point radius increases with the fire intensity [Adams, Williams, and Tregellas-Williams, 1972], and should also increase with the burning-zone dimensions. It is therefore assumed that the turning-region height is O(H) and

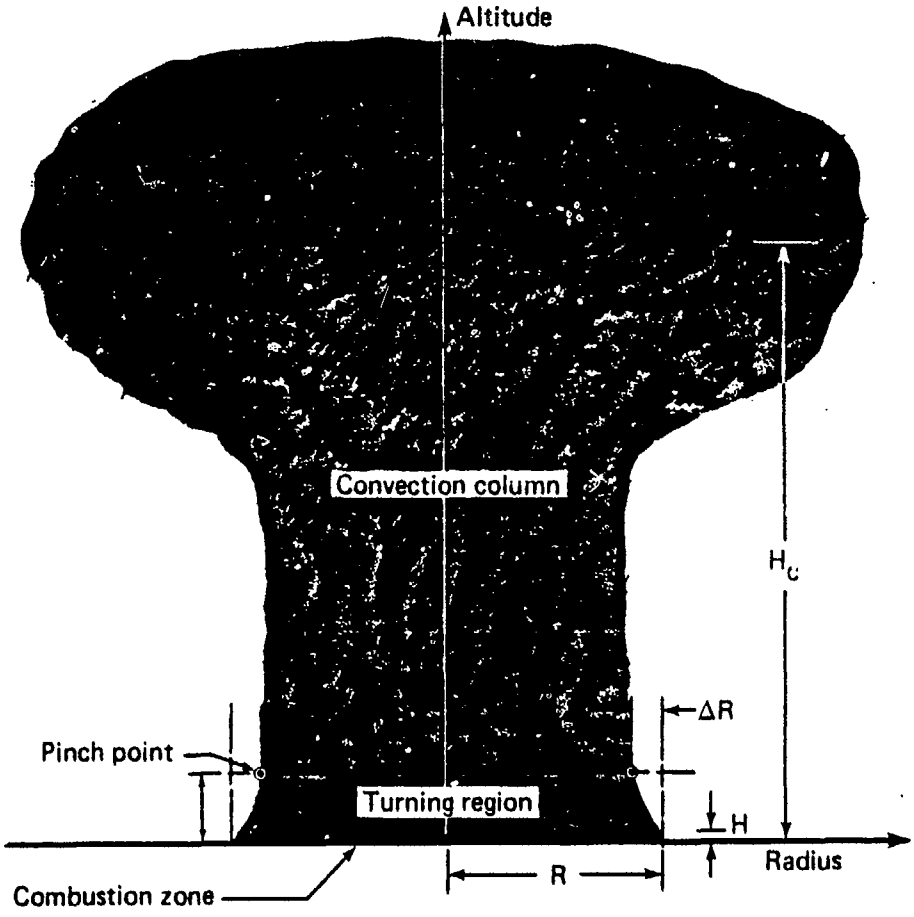

Figure 1. Schematic of large area fire system.

$$\Delta R < R \, . \qquad (2)$$

In general, a rigorous solution of a large area fire system should consider a coupled equation set that describes the hydrodynamics as well as the combustion dynamics. In this section, we limit the analysis to the hydrodynamics of a flow driven by strong buoyancy (fire) by modeling the combustion processes as an a priori defined, spatially dependent volume heat addition. The basic flow and thermodynamics, though dependent on the heat addition, are decoupled from the specifics of the combustion processes. The spatial function [see Eq. (8)] may be used to define areas of increased, limited, or no burning.

The specification of a heat addition rate implies that sufficient mass flow exists for combustion to be supported throughout the burning region. The built-up area of most cities rarely exceeds 40 percent of the available land, and street networks provide channels to bring "cold" air into the central regions of the fire. Thus, wide areas of burning may occur. The solution obtained must provide a mass flow consistent with the specified heat rate. Such values are obtained.

Consistent with the heat addition model, changes in gas composition resulting from the combustion chemistry are neglected. However, since large changes in temperature and density are expected, the Boussinesq approximation is not employed. The flow in the turning region is therefore taken to be that of an ideal, compressible gas undergoing heating in a finite surface layer.

There is some conjecture that, after long periods of time, ambient vorticity may be sufficiently concentrated to engender a rotating or swirling column [Long, 1967]. The rotation would in turn apply a biasing radial pressure gradient on the burning region and thus affect the rate of airflow into the fire. However, since only a few observations support that hypothesis, and strongly swirling columns are believed to be rare [Carrier, Fendell and Feldman, 1982], rotational forces are neglected in this analysis.

The experimental work of McCaffrey [1979] and the analyses of Murgai [1962] and Smith [1967] suggest that radiation from the heated

gas and attendant smoke plays an important role in reducing local air temperatures to nearly atmospheric within a few flame heights above the fire. Radiation losses as well as the effects of turbulent mixing are therefore included in the model, though in rather simple, qualitative ways. The radiation losses are assumed to occur in volume and to be "transparent" [Murgai, 1962]. Eddy diffusivities are used to describe the Reynolds stresses.

In a thin layer near the ground, a large vertical shear due to the no-slip requirement is expected. However, as distance from the surface increases, a predominately radial shear develops. The free-convection flow at the top of the turning region as well as the flow near the symmetry axis are characterized by such a shear. Mathematically, an analysis of the turning region should include a mechanism that permits radial propagation of information and allows the fire-wind inflow to depend on conditions in the center. Radial diffusion of momentum and energy provides such a mechanism. We thus focus on a parabolic formulation that considers a dominant radial shear.

At the fire periphery (radius ≈ R), steep gradients in temperature, pressure [Smith, Morton, and Leslie, 1975], and mixing coefficients are to be expected. Though they occur over distances much less than R, such rapid changes are critical in determining the more gradual variations over the entire width of the turning region. Since $\Delta R < R$, the radius of the turning region is taken to be R at all altitudes, and rapid changes in quantities around the periphery are idealized as jumps (discontinuities) at that radius. The magnitudes of such jumps are governed by standard statements of mass, momentum, and energy conservation. Outside the fire, the thermodynamic state is assumed to be that of the ambient atmosphere and turbulent stresses are of lower order.

Scalings and Basic Equations.

Leading-order predictions of the mean radial and vertical velocities u and v, temperature T, density ρ, and pressure P in the turning region are sought. The following nominal variable scalings (denoted by braces) are employed:

$$\{r\} = R\ ,\quad \{y\} = H\ ,\quad \{u\} = U\ ,\quad \{v\} = \varepsilon H\ ,$$
$$\{T\} = T_a\ ,\quad \{\rho\} = \rho_a\ ,\quad \{P\} = P_a\ , \tag{3}$$

where r and y represent radial and vertical positions, respectively; U is a radial velocity scale yet to be chosen; and T_a, ρ_a, and P_a represent ground-level atmospheric temperature, density, and pressure.

Since a subsonic flow is expected, pressure is rescaled using

$$\hat{P}/P_a = 1 + \delta P\ ,\quad \delta = U^2/P_a/\rho_a\ , \tag{4}$$

and we anticipate that $\delta < 1$. The leading-order set of conservation and state equations [Small, Larson, and Brode, 1981] is then

$$\frac{\partial}{\partial r}(r\rho u) + \frac{\partial}{\partial y}(r\rho v) = 0\ , \tag{5}$$

$$\rho\left(u\frac{\partial u}{\partial r} + v\frac{\partial u}{\partial y}\right) = -\frac{\partial P}{\partial r} + M_1\left[\frac{1}{r}\frac{\partial}{\partial r}\ r\frac{\partial u}{\partial r} - \frac{u}{r^2}\right] + M_2\frac{\partial^2 u}{\partial y^2}\ , \tag{6}$$

$$\frac{\partial P}{\partial y} + A\rho = 0\ , \tag{7}$$

$$\rho\left(u\frac{\partial T}{\partial t} + v\frac{\partial T}{\partial y}\right) = B\left[q(r,y) - \hat{\sigma}(T^4 - 1)\right] + K_1\left[\frac{1}{r}\frac{\partial}{\partial r}\left(r\frac{\partial T}{\partial r}\right)\right] + K_2\ \frac{\partial^2 T}{\partial y^2}\ , \tag{8}$$

$$\rho T = 1\ , \tag{9}$$

where

$$A = \frac{gH}{U^2}, \quad B = \frac{\gamma-1}{\gamma}\left(\frac{QR}{P_a U}\right),$$

$$M_1 = \frac{\varepsilon^{3-2i}\,\mathcal{C}_i}{\rho_a UH}, \quad K_1 = \frac{\varepsilon^{3-2i}\,k_i}{\rho_a c_p UH},$$

$$\hat{\sigma} = 4\pi\sigma k^* \frac{T_a^4}{Q} = 4\pi\sigma T_a^4 \left(\frac{k^* H}{QH}\right).$$

Here, Q is a scale for the rate of heat addition due to combustion and q(r,y) is a specified spatial distribution. The $\mathcal{C}_i$ and k_i are dimensional mixing coefficients, the specific heat capacity c_p is assumed constant, σ is Stefan's constant, and k^* is the reciprocal of the radiation mean free path (assumed constant).

In this formulation, the turbulence stresses are assumed to play a central role in determining the mechanics of the turning process. Inclusion of those terms produces an equation set that mathematically can duplicate the observed features of large fires. The solutions obtained confirm this hypothesis, at least for the simulations performed to date.

Specification of the relative magnitudes of the Reynolds' stress terms assumes that correlations for the fluctuating terms are known either on a theoretical or experimental basis. Test data are sparse and inconclusive (see, for example, Nielsen, 1970) and theoretical treatments are not available for the flows considered. Numerical solutions have used gradient transport approximations [Smith, Morton, and Leslie, 1975] (constant eddy diffusivity with the stress terms reduced to $K\nabla^2\phi$) and modified k - ε models [Markatos, Malin, and Cox, 1982; Markatos and Cox, 1984]. The latter calculations include the fire-generated flow in an enclosure; the former include a buoyant flow (generated by a boundary heat flux) in the atmosphere. Each approximation has its limitations when applied to a large area fire,

although the k - ε model intuitively seems more attractive--provided the needed empiricisms can be defined. In the absence of measurements, a range of eddy diffusivities has usually been assumed [Smith, Morton, and Leslie, 1975].

The specific correlation to be adapted depends on the rather qualitative appreciation of the flow processes dominating the turning region. In the burning region, a high-velocity radial flow is induced which stagnates at the centerline. A particle track may include local recirculations as well as passage through multiple flame regions, the net effect being a drag on the fluid. Similarly, in the axial direction, particles may be rapidly accelerated in flame regions yet also track local vortex or eddy motions.

The scalings applied to the Reynolds' stresses,

$$\bar{\rho}\,\overline{u'u'},\quad \bar{\rho}\,\overline{u'v'},\quad \bar{\rho}\,\overline{u'T'},\quad \bar{\rho}\,\overline{v'T'}, \tag{10}$$

assume that the fluctuating terms are each proportional to their mean component, i.e., $u' \sim \alpha_1 U$; $v' \sim \alpha_2 V$. Thus a strong anisotropy is postulated since $\overline{u'u'} \sim (1/\varepsilon^2)\overline{v'v'}$. In scaled variables, the stress terms involving $\overline{u'u'}$ and $\overline{u'v'}$ are of similar order and reduce to $M_1\,[(1/r)\partial/\partial r\,(r\partial u/\partial r) - u/r^2]$ and $M_2\,\partial^2 u/\partial y^2$. The M_1 and M_2 (and similarly K_1 and K_2) are probably of similar order (except near $r = 0$) in the burning region ($r,y \lesssim 1$). Above this region $M_2/M_1 \to 0$ consistent with the development of the free convection column. In the axial momentum balance, the stress terms $\partial(\overline{ru'v'})/\partial r$ and $\partial(\overline{v'v'})/\partial y$ are $O(\varepsilon)$ as are the inertia terms; whereas the pressure gradient and buoyancy terms are $O(1/\varepsilon)$.

An appropriate value for the horizontal velocity scale U is found by balancing the terms for convective transport and heat addition in the energy equation so as to properly represent the physics of a flow driven by combustion heating. Accordingly, we take $B = 1$ and find the characteristic fire-wind velocity to be

$$U = (\gamma - 1)QH/\gamma\varepsilon P_a\ . \tag{11}$$

For the sample fires considered in the "Results" section, areal heating rates (QH) and burning-zone aspect ratios (ε^{-1}) are on the order of 50 kcal/m^2-s and 30, respectively. The characteristic velocity scales are thus of order 20 m/s.

Boundary Conditions.

The type of boundary conditions to be used with Eqs. (5) through (9) depends on the nature of the energy and horizontal momentum equations, and hence on the relative magnitudes of the coefficients M_i and K_i, $i = 1,2$. A general model might assume that all such coefficients are of numerical order one. The energy and horizontal momentum equations would then be elliptic. Special cases arise, however, when M_1, $K_1 < M_2$, $K_2 \sim O(1)$ or M_2, $K_2 < M_1$, $K_1 \sim O(1)$. Equations (6) and (8) are then nearly parabolic.

We consider first the elliptic case, in which all mixing coefficients are of order one. At the ground,

$$u = v = 0 , \quad \mathfrak{F}(T, \partial T/\partial y) = 0 \quad \text{at } y = 0 . \tag{12}$$

In Eq. (12), $\mathfrak{F} = 0$ prescribes either a heat loss to the ground or a temperature distribution. Symmetry at the axis requires

$$u = \partial T/\partial r = 0 \quad \text{on } r = 0 . \tag{13}$$

In the upper part of the turning region, the flow approaches a nearly vertical, weakly buoyant state characteristic of the convection column. Since H is much less than the atmospheric scale height, the ambient temperature and pressure outside the turning region are

$$T_a[1 + o(1)] \quad \text{and} \quad P_a\{1 + \delta Ay[1 + o(1)]\} , \tag{14}$$

respectively [see Eqs. (3) and (4)]. Those conditions imply the following leading-order prescription for u, T, and P as $y \to \infty$:

$$u \to 0 \quad , \quad T \to 1 \quad , \quad P + Ay \to 0 \quad \text{as } y \to \infty \ . \tag{15}$$

The conditions in Eqs. (15) are formally derived [Countryman, 1969] from a matching of asymptotic expansions that describe, as $\varepsilon \to 0$, the separate turning-region and convection column flows.

Finally, in order to conserve mass, momentum, and energy across the fire perimeter, the magnitudes of effective jumps in physical quantities at $r = 1$ must satisfy certain conditions. Those jump conditions are easily found by writing Eqs. (5), (6), and (8) in conservation form and then integrating from $r = 1^-$ to 1^+. With jumps ($r = 1^-$ to 1^+) being denoted by [ ], the resulting conditions* are

$$\begin{aligned} [\rho u] &= 0 \ , \\ [\rho u^2] &= -[P] + [M_1 \partial u/\partial r] \ , \\ [\rho u T] &= [K_1 \partial T/\partial r] \ . \end{aligned} \tag{16}$$

To leading order, with mixing coefficients being much greater inside the turning region than outside, and atmospheric temperature being $T_a[1 + o(1)]$, yields:

$$\begin{aligned} T^+ &= \rho^+ = 1 \ , \\ [M_1 \partial u/\partial r] &= \bar{M_1}(\partial u/\partial r)^- \ , \\ [K_1 \partial T/\partial r] &= \bar{K_1}(\partial T/\partial r)^- \ , \end{aligned} \tag{17}$$

where $T^+ = T\big|_{r=1^+}$, etc. Thus, by integrating Eq. (7) along $r = 1^+$,

---

* Since Eq. (7) contains no derivative of r, the analogous jump condition is trivially satisfied and a consistent leading-order description is maintained.

$$P^+ = -Ay \ . \tag{18}$$

Using Eqs. (17) and (18), eliminating u^+ and using Eq. (9), the boundary conditions (Eqs. 16) applicable at the fire periphery ($r = 1^-$) are

$$M_1 \partial u/\partial r = (u/T)^2 (T - 1) + (P + Ay) \ ,$$

$$K_1 \partial T/\partial r = u(T - 1)/T \quad \text{on } r = 1 \ . \tag{19}$$

The primary elliptic boundary-value problem posed by Eqs. (5) through (9), (12) through (15), and (19) provides a model for the hydrothermodynamics of the turning region for the case where all M_i and K_i are of numerical order one. That model thus describes flows for which the effects of turbulent mixing are dynamically important in both the radial and axial directions.

We now consider the nearly parabolic case with M_1, $K_1 < M_2$, K_2, which is characteristic of flows having an axially dominant turbulent structure. In a fully parabolic analysis with $M_1 = K_1 = 0$, the boundary conditions in Eqs. (12) and (15) must be retained, but the symmetry conditions in Eq. (13) cannot be satisfied. In general, those symmetry conditions can be satisfied only through the development of an axial boundary layer in which horizontal mixing plays a leading-order role. Additionally, Eqs. (19) degenerate for $M_1 = K_1 = 0$ to the single condition $T = 1$. With no peripheral constraint being imposed in u, this parabolic analysis cannot yield a unique determination of the turning-region flow.

A well-posed boundary-value problem can be defined, however, for flows having a radially dominant turbulent structure, i.e., M_1, $K_1 > M_2$, K_2. In a fully parabolic analysis with $M_2 = K_2 = 0$, all boundary conditions in Eqs. (13) and (19) can be retained, so as to preserve the correct flow structure about the symmetry axis and at the fire perimeter. However, along $y = 0$, neither the no-slip condition on

velocity nor any condition on temperature can be enforced. The satisfaction of those conditions (Eqs. 12) requires the development of a thin surface layer in which vertical mixing plays an important role. Further, the only necessary condition in Eqs. (15) is that involving pressure. Equations (7) and (9) imply that, as $y \to \infty$, $\rho \to 1$ and $T \to 1$ if $P + Ay \to 0$. Thus, from Eqs. (6), (13), and (19), $u \to 0$. The proper set of boundary conditions for the case with $M_2 = K_2 = 0$ is therefore

$$v = 0 \quad \text{on } y = 0 , \tag{20}$$

$$u = \partial T/\partial r = 0 \quad \text{on } r = 0 , \tag{21}$$

$$P + Ay \to 0 \quad \text{as } y \to \infty , \tag{22}$$

$$M_1 \partial u/\partial r = (u/T)^2 (T - 1) + (P + Ay) , \tag{23}$$

$$K_1 \partial T/\partial r = u/T (T - 1) \quad \text{on } r = 1 . \tag{24}$$

Neglecting the axial diffusion of momentum and energy assumes that the buoyancy force, pressure gradients, and radial diffusion prescribe the leading-order development and decay of the flow. Retention of the radial diffusion terms defines a structure consistent with the developing column flow and couples the solution at all radii. With the exception of a thin, viscous layer near the ground, the parabolic boundary-value problem defined by Eqs. (5) through (9) and (20) through (24) with $M_2, K_2 = 0$ thus retains the essential physical features and structure of the elliptic model. Its solution, in the semi-infinite strip $r \leq 1$, $y \geq 0$, provides a description of the turning-region flow. The simplicity offered by this formulation allows demonstration of the principal interchanges of momentum and energy. In the following sections, solutions and results are presented for this parabolic case.

SOLUTIONS.

Closed-Form Solution for Weakly Heated Flows.

Before considering the general numerical solution of Eqs. (5) through (9) and (20) through (24) for M_2, $K_2 = 0$, it is instructive to examine the restricted case of a "weakly heated" flow, i.e., $q(r,y)$ small. For that case, a closed-form solution that summarizes the physical interactions in the turning-region flow can be derived. As an example, we consider

$$q(r,y) = \nu q_1(y) , \quad \nu < 1 ,$$

$$q_1(y) = \begin{cases} 1 & \text{for } 0 \leq y \leq 1 , \\ 0 & \text{for } y > 1 . \end{cases} \tag{25}$$

For weak heating, relatively small temperature changes and velocities are expected. Asymptotic expansions of the following type, valid as $\nu \to 0$, are sought for the solution of Eqs. (5) through (9), (20) through (25):

$$T \sim 1 + \nu T_1 + \ldots , \tag{26}$$

$$\rho \sim 1 - \nu T_1 + \ldots , \tag{27}$$

$$P \sim -Ay + \nu P_1 + \ldots , \tag{28}$$

$$u \sim \nu u_1 + \ldots , \tag{29}$$

$$v \sim \nu u_1 + \ldots . \tag{30}$$

In the $\nu \to 0$ limit, the leading-order problem obtained by substituting Eqs. (25) and (26) through (30) into Eqs (5) through (9) and (20) through (24) is then

$$K_1(1/r)\partial/\partial r(r\partial T_1/\partial r) + q_1(y) - 4\sigma T_1 = 0 , \tag{31}$$

$$\partial P_1/\partial y = AT_1 , \tag{32}$$

$$M_1[(1/r)\partial/\partial r(r\partial u_1/\partial r) - u_1/r^2] = \partial P_1/\partial r , \tag{33}$$

$$\partial v_1/\partial y = -(1/r)\partial/\partial r(ru_1) , \tag{34}$$

subject to

$$v_1 = 0 \quad \text{on } y = 0 , \tag{35}$$

$$u_1 = \partial T_1/\partial r = 0 \quad \text{on } r = 0 , \tag{36}$$

$$P_1 \to 0 \quad \text{as} \quad y \to \infty , \tag{37}$$

$$M_1 \partial u_1/\partial r = P_1 , \quad \partial T_1/\partial r = 0 \quad \text{on } r = 1 . \tag{38}$$

The problem posed by Eqs. (31) through (38) is readily solved. Equation (31) involves T_1 alone. Subject to boundary conditions (36) and (38), it must have a sclution that depends only on v. Once that solution is found, Eqs. (32), (33), and (34) are decoupled and solved in succession for P_1, u_1, and v_1. For $y > 1$, $q_1(y) \equiv 0$. The only solution of Eqs. (31) through (38) then satisfying Eqs. (36), (37), and (38) has T_1, P_1, u_1, and $\partial v_1/\partial y$ all zero. For $y > 1$, v_1 is thus a function of radius only, i.e., $v_1 \equiv v_1(r,1)$.

For $0 \leq y \leq 1$, $q_1(y) \equiv 1$ and it can be easily verified that the unique solution of the uncoupled boundary value problem for T_1 is $T_1 \equiv 1/(4\sigma)$. Formally, then, the solution for T_1 suffers a discontinuity at $y = 1$, which may be removed by using a boundary-layer-type solution about $y = 1$. Reconstructing Eqs. (20) through (24) using $\tilde{y} = (y - 1)/\nu$, it can be shown that P_1 and v_1 must be independent of $\tilde{y}$

over the boundary layer. The solution of Eqs. (31) through (34) for $0 < y < 1$ must therefore satisfy $P_1(r,1) \equiv 0$, and provide the $v_1(r,1)$ profile to be used for $y > 1$.

With $T_1 \equiv 1/(4\sigma)$ and $P_1(r,1) = 0$, the complete solution of Eqs. (31) through (38) for the fire zone is then found to be

$$T_1 \equiv 1/4\sigma \quad , \quad P_1 = -(A/4\sigma)\ (1 - y) \ ,$$

$$u_1 = (P_1/M_1)r = -(A/4\sigma M_1)\ (1 - y)r \ ,$$

$$v_1 = (A/2\sigma M_1)\ (y - y^2/2) \quad \text{for } 0 \leq y \leq 1 \ . \tag{39}$$

This solution summarizes the turning-region physics. The combustion heating [Eq. (31)] causes an increase in temperature and thus a decrease in density [Eq. (27)]. The mean pressure is then hydrostatically lowered [Eq. (32)], inducing the fire-wind inflow [Eq. (38)]. Finally, the inflow is kinematically turned upward [Eq. (34)], forming the initial part of the convection column.

Numerical Solution.

In general, the boundary value problem posed by Eqs. (5) through (9) and (20) through (24) must be solved by numerical computation. Subject to $M_2, K_2 = 0$, the differential equations (5) through (9) are either parabolic or first-order hyperbolic. Such equations are usually solved subject to initial conditions or certain combinations of initial and boundary conditions, but not subject to boundary conditions on all sides of the domain of definition, as prescribed in Eqs. (20) through (24). The boundary value problem is thus unusual, and a novel algorithm is employed to solve it numerically.

The solution procedure involves iteration toward the correct form of $P(r,0)$ [Small, Larson, and Brode, 1981]. A nonlinear Crank-Nicolson scheme [Isaacson and Keller, 1966] is used to obtain a numerical solution of Eqs. (5) through (9), (20), (21), (23), and (24) for $y > 0$. After the calculation is carried to some specified al-

titude y_{max} (> H), an error index

$$e = \max_{0 \le r \le 1} \left| P(r,y_{max}) + Ay_{max} \right| \tag{40}$$

is computed [cf. Eq. (23)]. For e greater than a specified tolerance, P(r,0) is corrected using the following simple iteration scheme:

$$P(r,0)_{new} = P(r,0)_{old} - \omega[P(r,y_{max}) + Ay_{max}] , \tag{41}$$

where ω is a specified relaxation coefficient. The prediction steps are then repeated until the process converges.

In practice, the scheme has proved to be stable and convergent--subject, of course, to reasonable initial values for P(r,0). For q(r,y) as in Eqs. (25), the resulting numerical solution reproduces the closed-form weak-heating solutions in Eqs. (26) through (30) and (39).

RESULTS.

The analysis presented in the preceding sections is formally valid for sufficiently large aspect-ratio (e < 1) fires. As sample calculations, a numerical simulation of a Flambeau fire and parametric excursions for larger area fires are presented.

Flambeau Experiments.

The Flambeau experiments were designed to model a large urban area fire. Those fires were instrumented for velocity, temperature, and weight-loss measurements. Documentary films provide visual data on flow patterns and plume development.

The largest Flambeau fires covered areas of about 20 ha, had flames rising up to 20 m, and produced heat release rates on the order of 10 to 100 kcal/m^2-s [Countryman, 1969; Palmer, 1981]. Maximum heat release is thought to have occurred in and around the fuel zone (height ~ 4 m), the heating decreasing with altitude above that zone. The experimental conditions are thus characterized by the following

parameters:* R = 250 m, H = 20 m, QH = 57 kcal/m^2-s, and

$$q(r,y) = \begin{cases} 1.6 & \text{for } 0 \leq y \leq 0.25 , \\ 1.6\,[4/3(1-y)] & \text{for } 0.25 \leq y \leq 1.0 , \\ 0 & \text{for } y \geq 1.0 . \end{cases} \qquad (42)$$

For these values $\varepsilon = 0.08$, the horizontal fire-wind velocity scale is $U = 8.41$ m/s, $\delta = 9.04 \times 10^{-4}$, and $A = 2.77$.

The required data set is completed by specifying the radiation mean free path $1/k^*$ and the turbulent mixing coefficients M_1 and K_1. Use of the transparent approximation [Murgai, 1962] assumes that $k^*H < 1$. However, Smith [1967] suggests that, for a turbulent flow, the effective absorption coefficient may be 30 to 80 times larger than the laminar absorption coefficient, implying k^*H could be of order one or larger. Since measurements supporting estimates of that parameter are not available for the fires considered, we select the nominal value $k^*H = 1$. Thus, $1/k^* = 20$ m and $\sigma = 0.022$. The one-parameter eddy-viscosity model of turbulence effects represents a gross simplification of the actual field turbulence. Because of a lack of correlations and relevant data, more detailed modeling does not seem warranted at this time. The eddy diffusivity is treated as a parameter and calculations are performed for several values. The sample results we now present were developed for $M_1 = K_1 = 4.0$, which corresponds to $\ell_1/\rho_a U = 1000$ m.

The results of the Flambeau simulation are illustrated by the streamline, contour, and profile plots in Figs. 2 through 7. The basic streamline pattern is shown in Fig. 2, and a more detailed view

---

*The specific value of QH here is suggested by Lommasson et al. [1968]. The form of q(r,y) is chosen to satisfy the normalization

$$\int_0^1 \int_0^1 rq(r,y)\, dr\, dy = \frac{1}{2} ,$$

which holds if $q \equiv 1$.

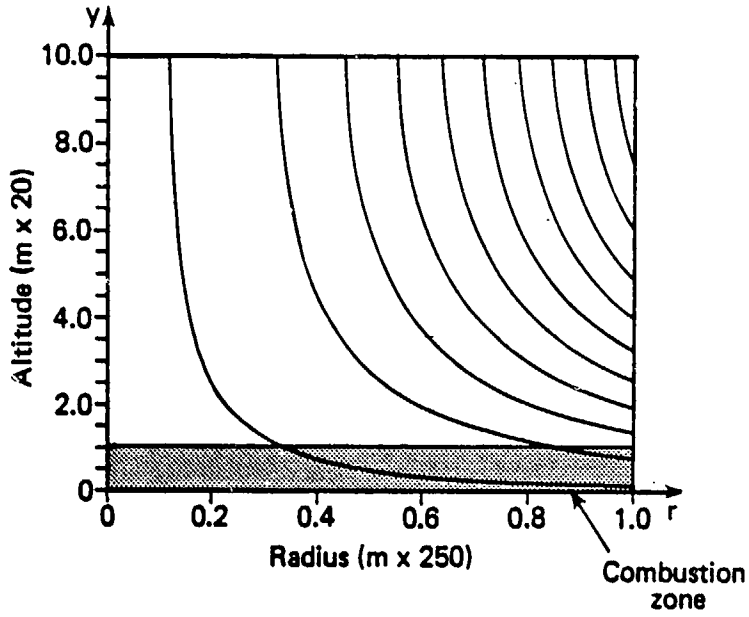

Figure 2. Streamline pattern for Flambeau fire.

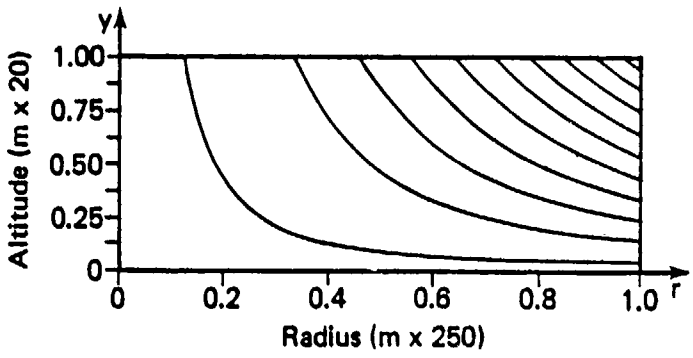

Figure 3. Streamline pattern for Flambeau combustion zone.

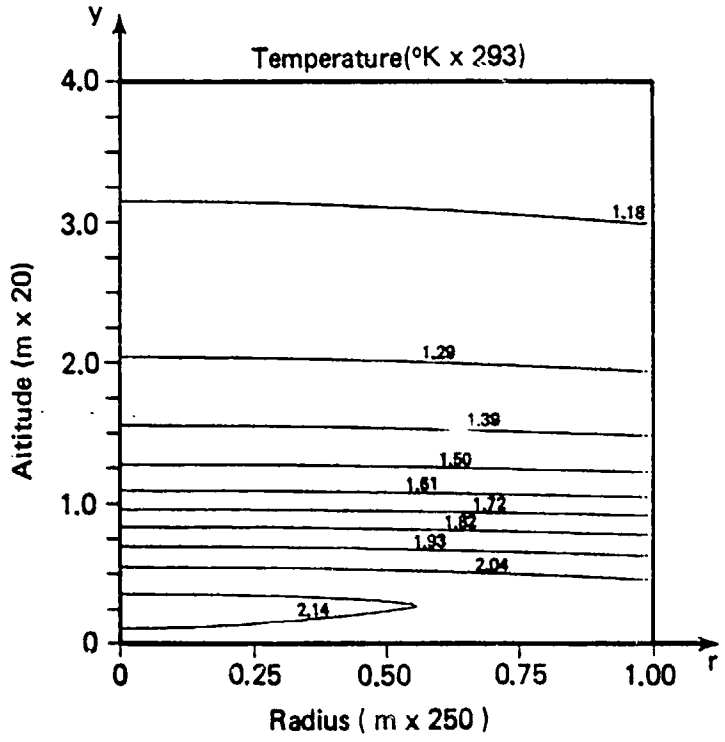

Figure 4. Temperature contours for Flambeau fire.

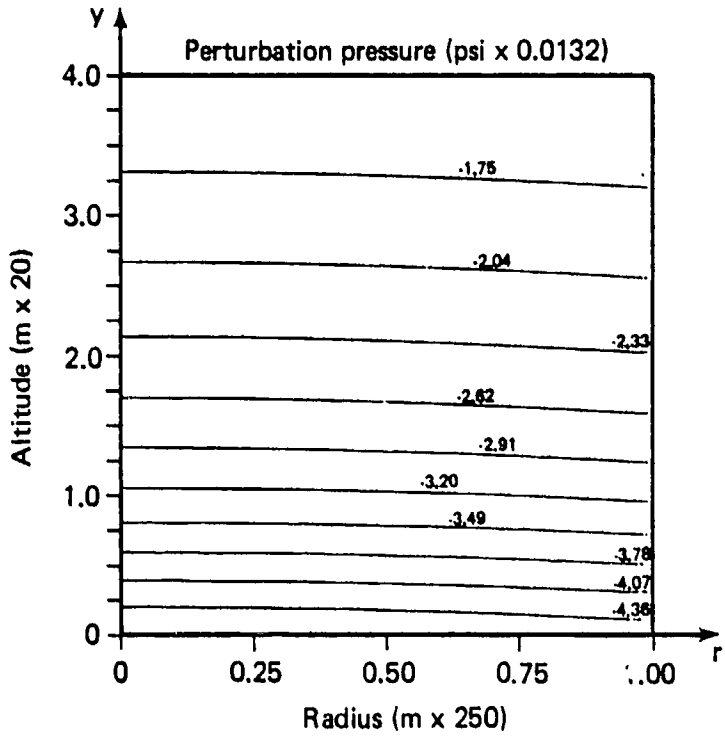

Figure 5. Pressure contours for Flambeau fire (perturbation pressure is δP_a (P + Ay).

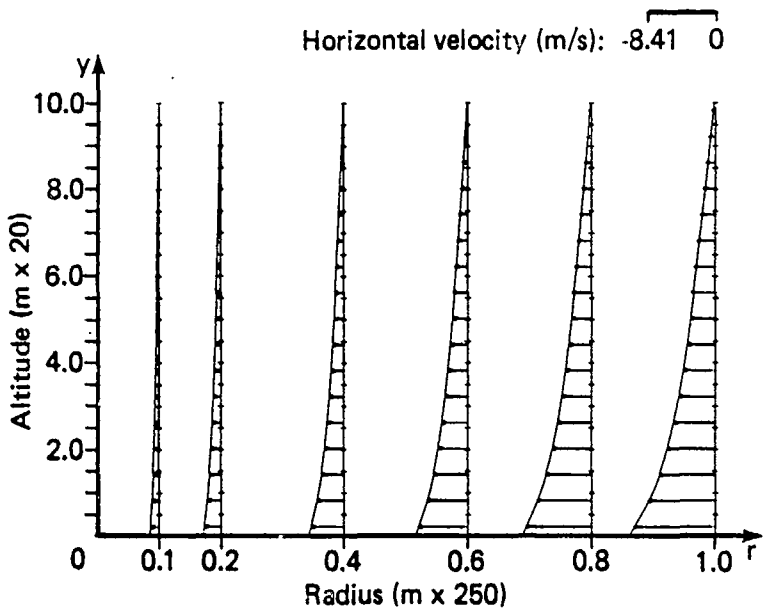

Figure 6. Radial velocity profiles for Flambeau fire.

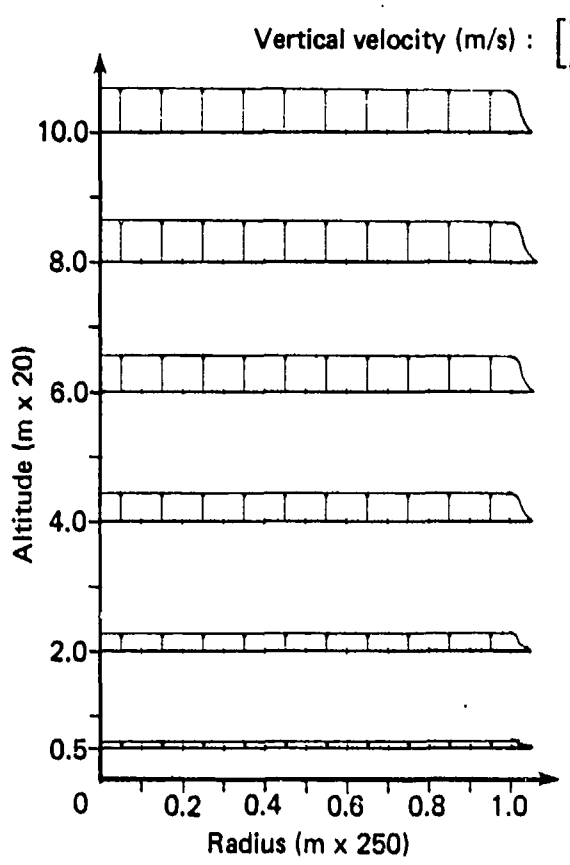

Figure 7. Axial velocity profiles for Flambeau fire.

(stretched in the vertical direction) is shown in Fig. 3. In the burning zone, the flow is largely horizontal, though the strong buoyancy forces a significant streamline curvature. Above eight flame heights, a nearly vertical flow is established.

The temperature rise and subsequent pressure drop in and arcund the fire due to combustion heating are shown in Figs. 4 and 5, respectively. The temperature reaches a maximum of 637 K at the center of the combustion zone. However, it then decreases rapidly with increasing height, attaining a state of weak buoyancy above an altitude of 100 m. Pressure is almost independent of radial range, except, of course, at the turning-region periphery. Such behavior is also characteristic of the more global computational results presented by Smith, Morton, and Leslie [1975]. The maximum pressure drop at the periphery occurs at ground level, and is 0.060 psi.

Figure 6 illustrates the nature of the basic horizontal inrush induced by the overall pressure drop. The maximum fire-wind inflow velocity at the periphery also occurs at ground level, and is 9.3 m/s. The resultant upward flow consistent with the induced inflow is shown in Fig. 7. Vertical velocity profiles are all nearly "top hat," with $v \approx 4$ m/s at the top of the turning region. The centerline velocity shows a rapid, nearly linear increase in the turning region, and then a slower increase with altitude. For $y \gtrsim 7$, the velocity approaches a constant value consistent with the initial convection column velocity. Such behavior is similar to that observed above small fires [McCaffrey, 1979].

In general, quantitative comparisons with Flambeau measurements are hindered by measurement scatter and the probability of error. Howe"er, a number of qualitative comparisons can realistically be made; in those cases, the predictions match the observed physical phenomena. The induced fire-wind profile (Fig. 6) and the subsequent flow pattern (Fig. 2) are consistent with filmed observations [U.S. Forest Service, 1967]. The horizontal inflow is turned strongly upward in a layer depth O(H), with a nearly vertical convection column flow forming several flame heights above the fire. Additionally,

predicted inflow velocities at the periphery and predicted temperatures agree with reported values [Countryman, 1969].

Parametric Analysis of Large-Fire Environment.

For a given volume heating distribution $q(r,y)$, the solution depends on four parameters: A, M_1, K_1, and $\hat{\sigma}$. The combustion zone dimensions R and H and the mean heating density Q specify the scale velocity U and the Froude number A^{-1}. The radiation mean free path $1/k^*$ and the eddy coefficients $\mathcal{C}_1$ and k_1 define the degree of heat loss ($\hat{\sigma}$) and the diffusive characteristics (M_1, K_1) of the flow. In general, for a given fire, the latter three parameters must be estimated. This section explores the solution dependence on combustion zone dimensions, heating rate, degree of turbulent mixing, and radiation.

A 10-km fire (see Table 1) with a heat distribution given by Eq. (42) is chosen as a baseline. Velocity profiles and thermodynamic contours are shown in Figs. 8 through 10.

Table 1. Parameter dependence on fire radius.

R(km)	U(m/s)	A	$\hat{\sigma}$	M_1, K_1
2.5	16.8	3.4720	0.1100	3.200
5.0	33.6	0.8680	0.1100	0.800
10.0	67.2	0.2170	0.1100	0.200
15.0	100.8	0.0964	0.1100	0.089
20.0	134.4	0.0534	0.1100	0.050

NOTE: QH = 57.4 kcal/m^2-s, H = 100 m.

The development of the vertical velocity profiles (Fig. 8) appears to correlate with the temperature (buoyancy) and pressure contours exhibited in Figs. 9 and 10. The flow achieves a state of weak buoyancy above three flame heights and a nearly vertical flow at

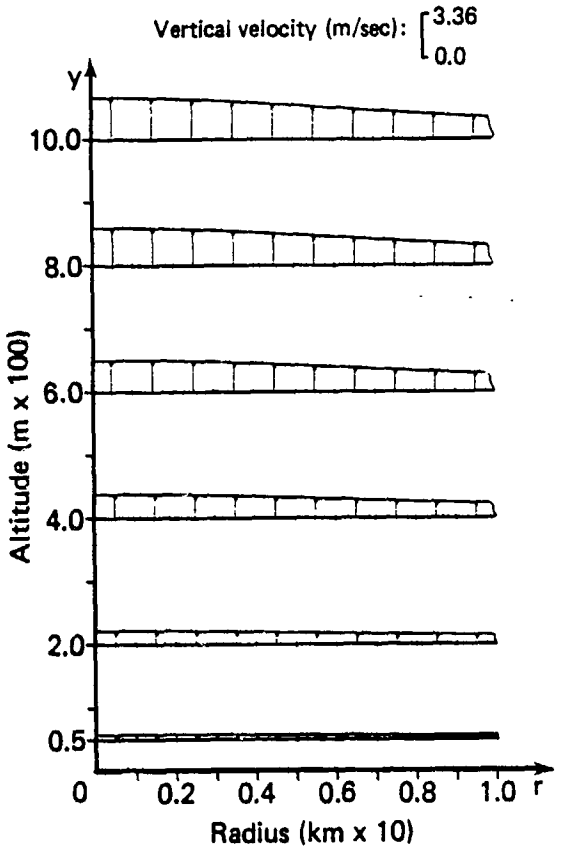

Figure 8. Axial velocity profiles for baseline fire.

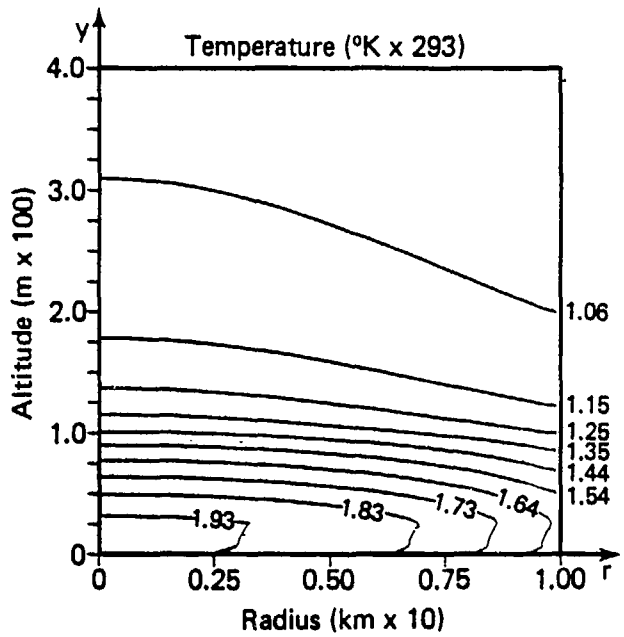

Figure 9. Temperature contours for baseline fire.

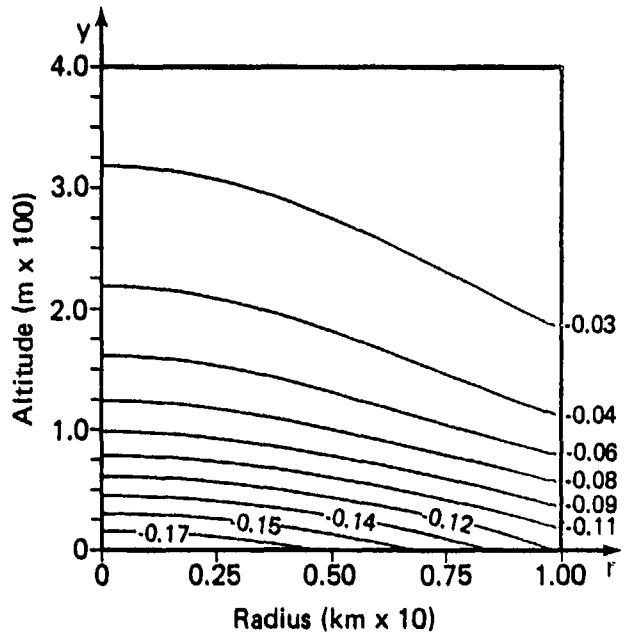

Figure 10. Pressure contours for baseline fire.

approximately eight flame heights. In most of the parameter excursions, qualitatively similar flows are observed.

The solution dependence on fire radius (Table 1) is shown in Figs. 11 and 12. The maximum radial velocity initially increases with fire radius and then asymptotes toward a constant value at larger radii. The temperature variation exhibits a similar behavior at large radii. This indicates a fire-wind dependence on the production of buoyancy per unit area. Relatively small changes in the maximum perturbation pressure are calculated.

The influence of changes in the heat addition rate (see Table 2) is explored in Figs. 13 and 14. As expected, the temperature (and, similarly, the pressure perturbations) increase with QH. The maximum radial velocity initially shows a rapid increase, but then slows for further increases in the burning rate (QH > 35 kcal/m^2-s).

Table 2. Parameter dependence on burning rate scale.

QH (kcal/m^2-s)	U (m/s)	A	$\hat{\sigma}$	M_1, K_1
14.35	16.8	3.4720	0.4400	0.80
28.70	33.6	0.8680	0.2200	0.40
57.40	67.2	0.2170	0.1100	0.20
86.10	100.8	0.0964	0.0825	0.15
114.80	134.4	0.0534	0.0550	0.10

NOTE: $R = 10^4$, $H = 10^2$ m.

The strong dependence on heating zone height (see Table 3) with both the radius and total heat addition (QH) fixed is exhibited in Figs. 15 and 16. Increasing H (flame height) lowers the energy density and hence the mean temperature. (Similarly, the mean pressure differential changes rapidly with H.) Despite the increase in temperature levels, the buoyancy force per unit area increases, implying larger fire-wind velocities. The solution's strong dependence on H

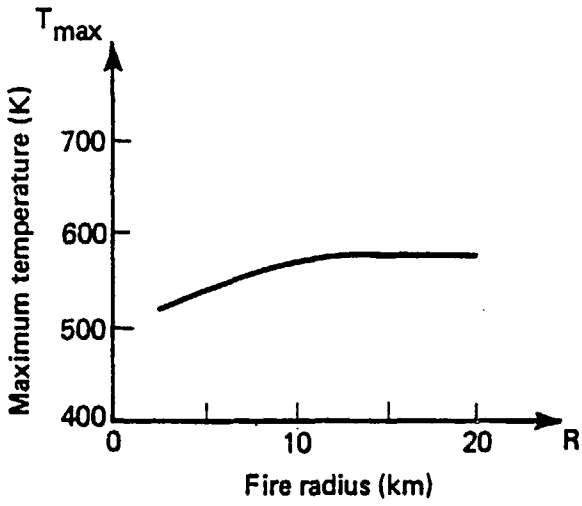

Figure 11. Maximum temperature versus fire radius.

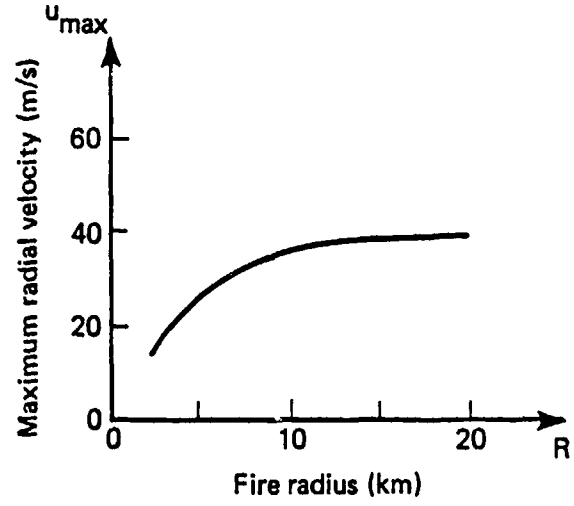

Figure 12. Maximum radial velocity versus fire radius.

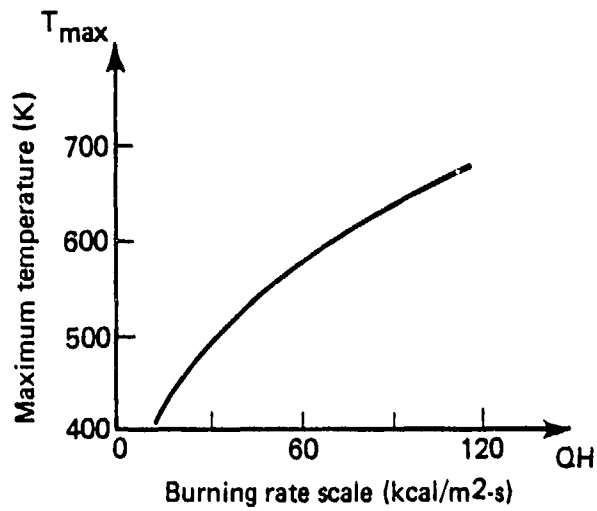

Figure 13. Maximum temperature versus burning rate scale.

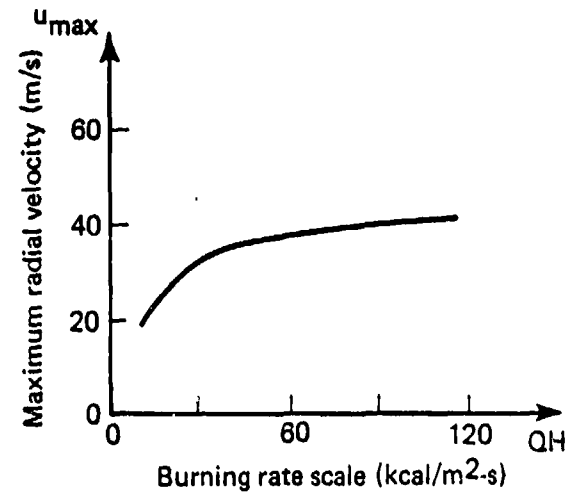

Figure 14. Maximum radial velocity versus burning rate scale.

suggests that hydrocode simulations of a large fire should use a volume heat source rather than a prescribed thermal condition at the ground.

The final parameter variations consider the influence of eddy coefficients and radiation mean free path on the solution. The heat addition rate and the combustion zone radius and height are held fixed at 57.4 kcal/m^2-s and 10^4 m, respectively. Figure 17 shows the effect of the eddy coefficients on the maximum fire-wind velocity. An increase in the effective viscosity (lower Rayleigh number) lowers the velocity. The temperature varies only slightly, however, being controlled for the most part by the heat addition and radiative loss. The turbulent diffusion of momentum dominates the response. Variation of the heat transfer coefficient with the eddy viscosity fixed produces only small changes in the maximum temperature, pressure, and velocity. The dependence of the maximum fire-wind velocity on the radiation mean free path is shown in Fig. 18. An increase in the mean free path effectively reduces the radiative loss of energy.

Table 3. Parameter dependence on fire height.

H(m)	U(m/s)	A	$\hat{\sigma}$	M_1, K_1
50	134.4	0.0272	0.055	0.4
100	67.2	0.2170	0.110	0.2
200	33.6	1.7360	0.220	0.1

NOTE: R = 10^2 m, QH = 57.4 kcal/m^2-s.

The corresponding increase in temperature implies a greater production of buoyancy and, in turn, a greater pressure gradient and inflow velocity.

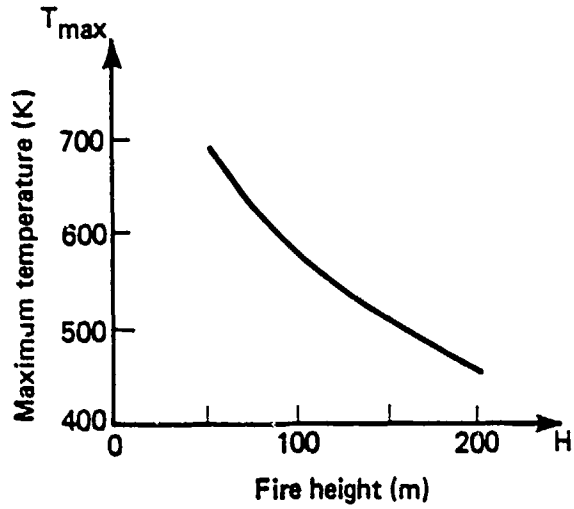

Figure 15. Maximum temperature versus fire height.

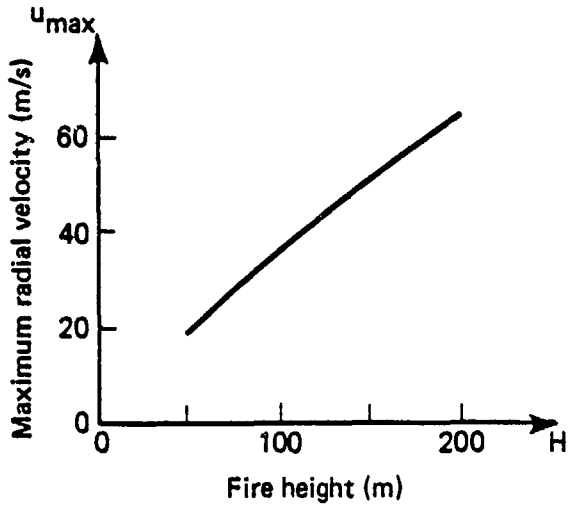

Figure 16. Maximum radial velocity versus fire height.

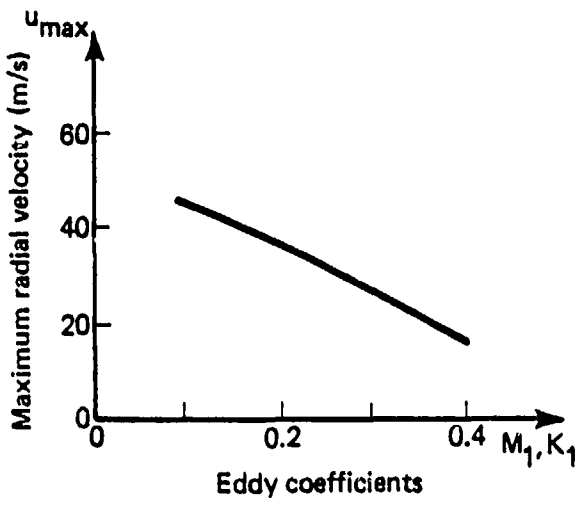

Figure 17. Maximum radial velocity versus eddy coefficients.

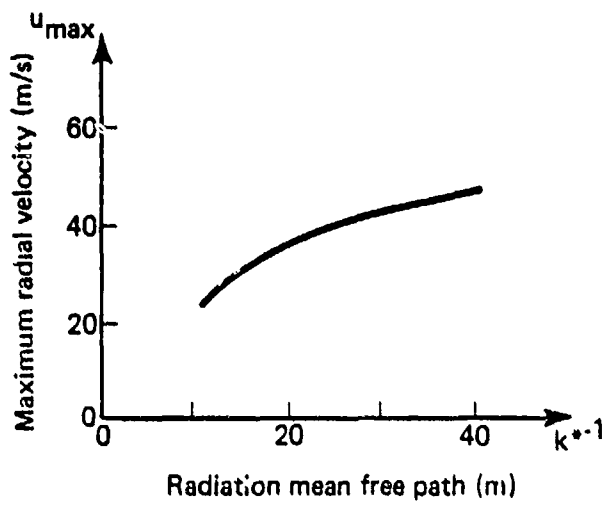

Figure 18. Maximum radial velocity versus radiation mean free path.

DISCUSSION.

The model developed here describes the velocity and thermodynamic fields generated by a large-aspect-ratio fire. The analysis focuses on the turning region, which includes the burning zone and the region below the established free-convection column. To leading order, the solution is independent of both the far field and the properties of the convection column. Although subject to some simplifying assumptions, the results of the analysis clearly illustrate the complex interactions occurring in the turning region.

The analytical procedure employs asymptotic methods to simplify the basic equations of momentum and energy conservation. A finite-volume heat source is used to model the combustion processes, and large changes in temperature and density are allowed. A one-parameter eddy-viscosity model is used to describe the turbulence stresses, and the transparent approximation employed to model hot gas and smoke radiation. Jump conditions are derived to describe the rapid changes in physical quantities at the fire periphery. Those conditions affect model problem closure, allowing the induced fire winds to be calculated directly, without extensive far-field computations.

The use of one-parameter models to represent the combustion processes, turbulent exchanges, and radiative heat transfer simplifies the analytical formulations, but such models of course only approximate the complex phenomena. Experimental definition of the turbulence properties of a large area fire would allow more detailed modeling.

A closed-form solution to the relevant boundary-value problem is developed for the restricted case of weak heating. That solution reveals the structure of the general solution, and concisely shows how the heating, production of buoyancy, pressure gradients, induced fire winds, and formation of the initial free-convection column are related. Those relationships are also evident in the sample numerical simulation of the strongly heated Flambeau fire. At the fire periphery, the temperature increases rapidly, generating steep pressure gradients and high-velocity fire winds. The inrush is turned upward by the buoyancy all along the burning zone, and forms the base

of a free-convection column in the upper portion of the turning region. The gas temperature increases slightly toward the center of the fire, but falls rapidly with height above the burning zone.

The parameter excursions illustrate the solution dependence on heating zone dimensions, combustion rate, and exchange coefficients. In general, the induced fire winds increase with the buoyancy production per unit area and the effective Rayleigh number. The turning-region flow is strongly controlled by the amount of heat addition and the degree of momentum diffusion.

SECTION 2
PHYSICS OF LARGE FIRES

There have been numerous occurrences of large area fires in urban centers. When whole areas have burned simultaneously, unusual and extreme conditions have resulted. Survivors of the "fire storms" at Hamburg, Dresden, Hiroshima, and other cities cite similar experiences. Extreme temperatures, even in the streets, and very high velocity fire winds were reported. Despite interpretations of the "data" that infer enhanced levels of ambient vorticity, unusual weather conditions, etc., it is principally the high temperatures and fire-wind velocities that are common to all the reported large fires.

In this section, we explore several analytic viewpoints that attempt to provide an explanation for the phenomena reported in World War II city fires, and to predict what might occur for a large-yield nuclear attack on an urban area. Our basic premise is that the ignition of fires over a large area, causing the release of energy in a volume representative of the flaming region, produces a distribution of buoyancy, which is the important feature to be modeled [Small and Larson, 1984; Small, Larson, and Brode, 1984]. The buoyancy from large fires initiates a chain of interrelated effects. Pressure gradients are generated and, as a consequence, a broad upward motion supported by a high-velocity inward flow (the fire winds) is induced [Smith, Morton, and Leslie, 1975; Cox and Chitty, 1980; Zukoski, Kubota, and Cetegen, 1981]. This simple view neglects many important transient features of large fires. Nevertheless, analyses of the flows generated by simple volume heat additions do explain many of the observed phenomena. Higher velocities could occur if a swirling column develops from, for example, topography, ambient wind shears, or fire-generated entropy gradients. In general, motions resulting from the strong buoyancy account for the high-velocity fire winds.

From our analyses, it appears that the World War II large city fires, as well as those that might result from nuclear weapon explosions over urban areas, are different from small laboratory-scale

fires or isolated building fires. In the large World War II fires, it was noted that all combustibles were consumed. That is seldom the case for ordinary building fires or fires involving several buildings or even several blocks, and suggests very intense burning across the entire area. Furthermore, fires with radii approaching 5 to 10 km have plumes almost as wide as their height. In fact, for low inversion or strong cross flows, the plume may have greater radial extent than vertical dimension.

Our study suggests that to analyze large area fires at least three features must be considered. First, plume motions are directly derived from fire dynamics, and therefore the fire source must be modeled in some detail. Resolution of details in this region is reflected in the distribution of buoyancy and hence in the plume structure. A point source (virtual origin) or thermal boundary condition (as opposed to a volume heat source) is apparently inadequate.

Second, since a plume is likely to be fairly broad relative to its height, edge entrainment is not a major factor influencing the plume equilibrium in the atmosphere. The usual similarity-type solutions are not appropriate for a broad plume. A plume whose dynamics are affected only slightly by Taylor-type entrainment is in contrast to thin plumes above small fires.

Third, plumes above large area fires are more seriously influenced by atmospheric gradients, inversion heights, and upper atmosphere crosswinds.

Our approach in the analysis of large fires has been to model the fire region (analytically) in some detail, and to calculate (in numerical experiments) the atmospheric response to large heat additions in finite surface volumes.

The source region analysis relates the heat addition to the production of buoyancy and to the induction (and turning upward) of the fire winds. The analysis is quasi-steady, restricted to very large aspect ratio fires, and valid only in the vicinity of the fire. Even though transient features are neglected, this analytical view provides some insight into the principal persistent features of large

fires. In addition, the analysis guides the formulation of the subsequent numerical experiments.

Time-dependent solutions describing the larger scale fire atmospheric motions are presented later. An axisymmetric solution for a 10-km radius fire in a quiescent (U.S. Standard) atmosphere is given. Solutions for a smaller fire in a crosswind (Flambeau) are also presented.

Notable in the hydrocode solutions are complex transient motions. Some local vortex motions account for periodically high centerline velocities; other vortices influence the ambient air induction from the far field and the plume rise. These vortex motions vary with time, especially in the early phase of the fire. Nevertheless, there is a uniformity and an overall persistence to the flow.

The calculated plume motions show that the atmosphere plays a major role in the equilibrium height attained by the fire products. In both calculations, lofting is limited. In the 10-km fire, the tropopause effectively capped the flow. For the Flambeau simulation, a 10 m/s crosswind turned the plume at approximately 3500 m--well below the tropopause.

Both the steady-state source region analysis and the time-dependent numerical simulations portray reasonable flow fields. There are, however, a number of simplifications and assumptions contained in both models. That there is reasonable agreement between simulation and experiment (as well as theory and observation), lends confidence to the models. Nevertheless, it is important to recognize deficiencies, as well as indicate processes such as turbulence, radiation, and heat release that require better description. Those issues are addressed in the "Discussion" section, p. 52.

ANALYTICAL VIEW OF LARGE AREA FIRES.

For asymptotically large fires, the ratio of the mean heat addition height (H) to fire radius (R) forms a small parameter:

$$\varepsilon = \frac{H}{R} , \quad \varepsilon << 1 , \tag{43}$$

which can be used to develop a simplified source region equation set. The major effects such as volume heat addition, radiative transfer, compressibility, and turbulence can be modeled--at least approximately--and included in the source description. Such an asymptotic analysis [Small and Larson, 1984; Small, Larson, and Brode, 1984] results in the following simplified equation set [similar to Eqs. (5) through (9) but with $M_2 = K_2 = 0$]:

$$\frac{\partial}{\partial r}(r\rho u) + \frac{\partial}{\partial y}(r\rho v) = 0 , \tag{44}$$

$$\rho\left(u\frac{\partial u}{\partial r} + v\frac{\partial u}{\partial y}\right) = -\frac{\partial P}{\partial r} + M_1\left[\frac{1}{r}\frac{\partial}{\partial r}\left(r\frac{\partial u}{\partial r}\right) - \frac{u}{r^2}\right], \tag{45}$$

$$\frac{\partial P}{\partial y} + A\rho = 0 , \tag{46}$$

$$\rho\left(u\frac{\partial T}{\partial r} + v\frac{\partial T}{\partial y}\right) = q(r,y) - \hat{\sigma}(T^4 - 1) + K_1\left[\frac{1}{r}\frac{\partial}{\partial r}\left(r\frac{\partial T}{\partial r}\right)\right], \tag{47}$$

$$\rho T = 1 . \tag{48}$$

In this formulation, all variables are O(1). The radial and axial coordinates are scaled with R and H, respectively.

Some insight into the interactions governing the flow is possible by inspection. The energy addition [Eq. (47)] raises the temperature; and thus decreases the density [Eq. (48)]. The resultant buoyancy field ($\Delta\rho$) induces pressure gradients [Eq. (46)] that in turn generate the radial fire winds [Eq. (45)]. The initial plume structure is then prescribed [Eq. (44)]. Except for restricted cases [see Small and Larson, 1984], the equations are coupled and require numerical solutions. Jump conditions [Eqs. (23) and (24)] are used to couple the ambient and fire regions.

This boundary value problem is easily solved on a minicomputer. The solutions illustrate the basic features of strongly buoyant fire generated flows, and provide insight into the influences of differing

heat rates, turbulence levels, radiative transfers, and fire sizes. Sample results shown in Figs. 8, 9, 12, 14, and 16 approximate the magnitudes to be expected in the time-dependent solution. Of special note is the effect of fire height (flame height or the volume in which heat is generated) on the induced fire winds (Fig. 16). The winds rise by a factor of 3 for a fourfold increase in effective flame height [see Small and Larson, 1984]. In the limit of zero height, the strength of the buoyancy field is limited by the diffusion of energy from the surface, and is greatly reduced. Thus, modeling the plume dynamics and the motions induced in the atmosphere requires careful resolution of the source region--despite the greater scale lengths involved in the dimensions of the plume and atmosphere.

TIME-DEPENDENT SOLUTIONS.

Only a limited number of solutions of the compressible, time-dependent conservation equations for the atmospheric motions generated by a large area fire have been reported [Smith, Morton and Leslie, 1975; Nielsen, 1970; Luti, 1981; Rosenblatt, 1983]. In each case, some simplifications (e.g., isothermal boundary rather than a volume heat input, no radiative losses, Boussinesq approximation) are introduced. The greatest restrictions usually apply to the fire and near-fire regions where the flow is compressible and energy transfers dominate. In general, each region (fire, central plume, plume top, far field) is expected to influence the overall solution. The formulation is elliptic; resolution of each flow regime is required.

The solution algorithm employed is based on a modified version of the simplified arbitrary Lagrangian-Eulerian (SALE) method [Amsden, Ruppel, and Hirt, 1980]. The principal modifications include the addition of a volume heat release source function, radiation loss model, variable eddy viscosity, and an implicit solution procedure for the energy equation. An ideal gas is assumed; chemistry is not included.

The neglect of chemistry as well as the influence of the local hydrodynamics on the heat release are important omissions. Nevertheless, rather than assume a thermal boundary condition, it seems

appropriate to account for the volume distribution of buoyancy--if only in a primitive manner.

Since fires of radii up to 10 km are considered, the solution domain extends to the stratosphere (30 km), and radially to 100 km (≈ 10 fire radii). In this volume, the fire (modeled as a prescribed heat release) is in a 10-km radius by 100-m height region. Accordingly, a nonuniform zoning is used.

The solutions for a 10-km radius fire, shown in Figs. 19 through 28 were obtained using a 47 (radial) by 61 (axial) point grid. The heat addition region contains 3 cells (vertically) by 20 cells (radially). The relatively fine grid in altitude (61 points) reflects the importance of atmospheric gradients on the dynamics of the plume and its ultimate equilibrium in the atmosphere. The U.S. Standard Atmosphere (with an 11-km tropopause) models the pressure-temperature altitude variation.

The example solutions were obtained for a uniformly applied heat addition rate of 1 kW/m^3. Representing the development of an intense area fire from a multitude of ignitions, the energy addition is increased linearly from zero to 1000 J/m^3-s in the first 15 min and then held constant. An eddy viscosity of 1000 m^2-s was assumed for the heat addition region, and 100 m^2-s elsewhere. This division, although arbitrary, recognizes the greater turbulence levels characteristic of a burning urban area.

At early times ($t \leq 15$ min), a series of essentially local flows (Figs. 19 through 21) are established in and near the heat region. Temperature increases are moderate (≈ 100 K) and several weak vortex motions develop across the region. The most pronounced motions are observed at the fire edge, where sharp temperature-density gradients are established, and also at the symmetry axis.

As the buoyancy field strengthens with the continued head addition, pressure gradients are established, and a radial inflow develops. At $t = 15$ min, the flow extends to 15 km. Replacement of the relatively weak initial roll motions by a strong inwardly directed flow begins. Two vortex motions remain, however, and strengthen with time. The strong vortex located near the fire boundary grows

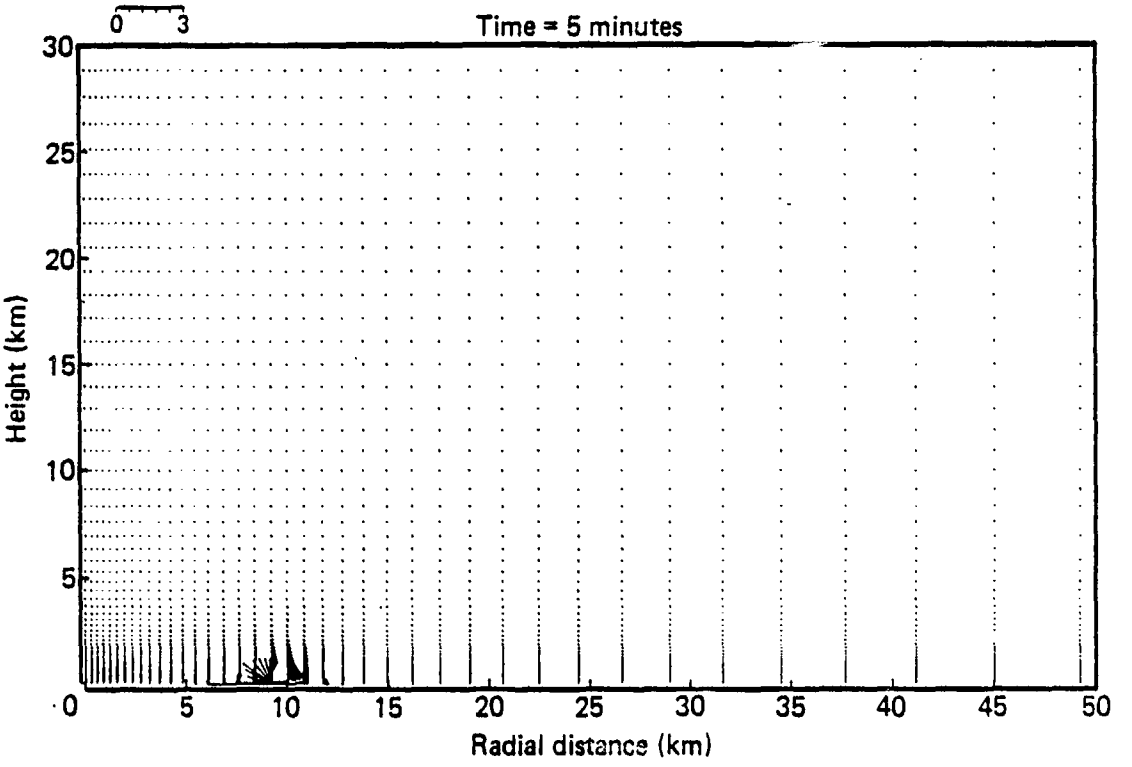

Figure 19. Velocity field generated by 10-km radius area fire at t = 5 min.

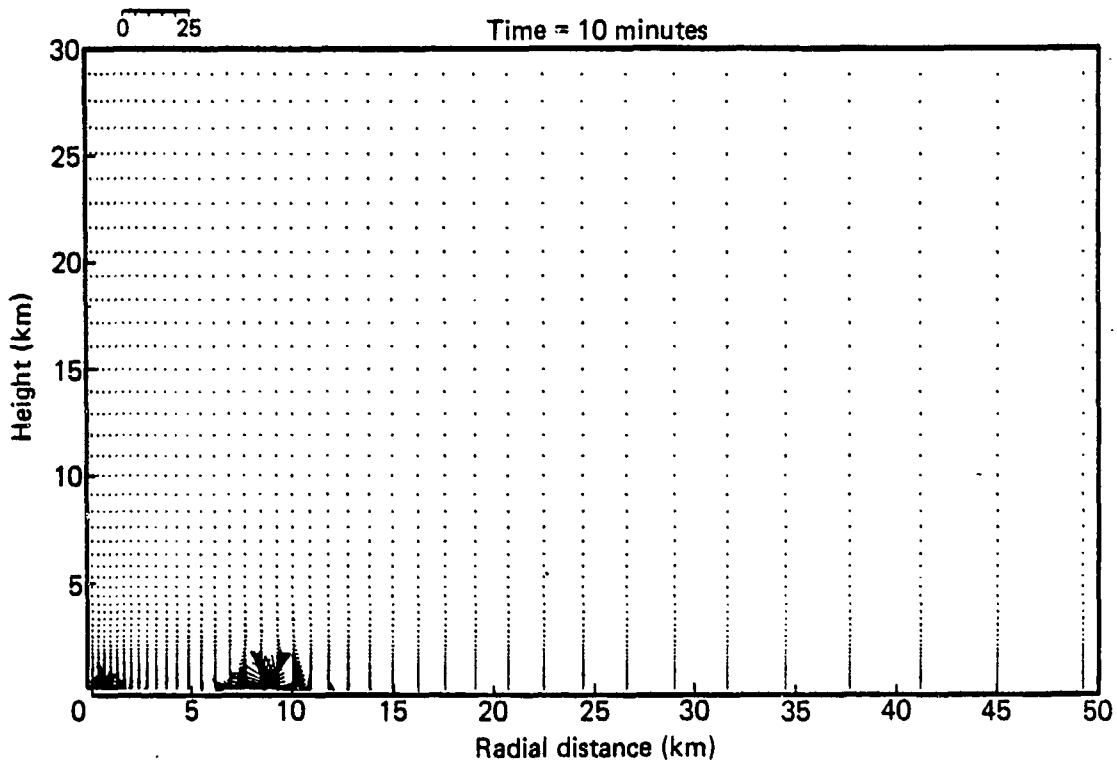

Figure 20. Velocity field generated by 10-km radius area fire at t = 10 min.

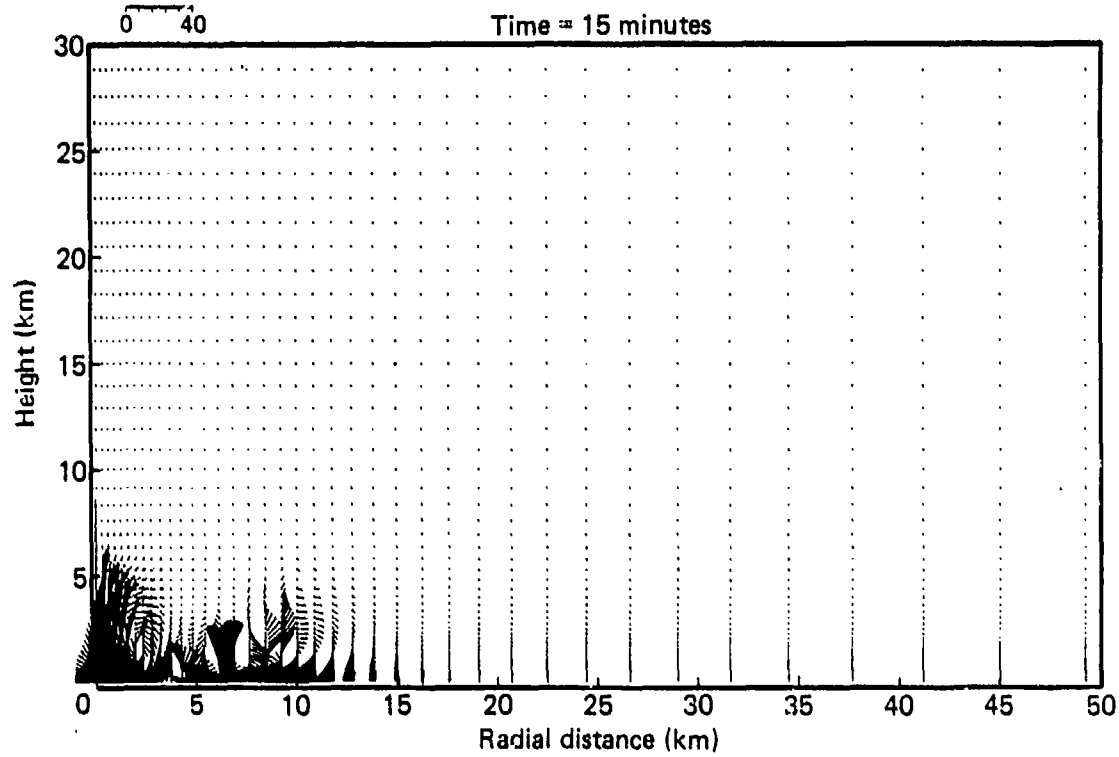

Figure 21. Velocity field generated by 10-km radius area fire at t = 15 min.

considerably, and at later times becomes a controlling feature of both the inflow and the plume rise in the atmosphere. The cellular motion near the symmetry axis contributes equally to the later flow dynamics. This initial corner vortex is stretched and convected axially. As a result, relatively high velocities develop on the centerline and persist until atmospheric gradients force cell breakup. Consequently, combustion products from the center are lofted through the tropopause for brief periods. Those motions are repeated as the flow system evolves. The periodic intrusions into the stratosphere may be enhanced by moisture condensation but suppressed by winds aloft; neither factor is accounted for in this solution.

Other solutions (not shown) obtained using larger zones (in the axial direction and for the heat addition region) do not show similar flows. A coarser grid solution (e.g., 200-m heat zone) produced a narrow--high velocity--axial plume that readily penetrated the tropopause, and probably the stratosphere, if the domain is sufficiently extended. Although the optimum zoning remains to be determined, the results suggest that finer grid representations are more appropriate.

Several views of the "mature" flow field are shown in Figs. 22 through 28. Although a steady flow does not develop, some persistent features are noted. Temperatures are relatively constant with time across the burning region, varying principally with height. The rapid change at the fire periphery is consistent with the jump conditions of Eqs. (23) and (24). Similarly, the buoyancy field and pressure gradients are relatively constant with time. Exceptions do occur when local vortex motions move cooler air into the heat-addition region. The more or less constant radial inflow indicated in the vector and streamline plots reflects the apparent steadiness of the "source function."

The inflow is also influenced by the strong vortex, which originates at the fire edge and which is located exterior to the burning region (see Figs. 22 through 28). A second (clockwise) cell located above the fire region strongly influences the rising and turning of the plume. Although additional motions are apparent at

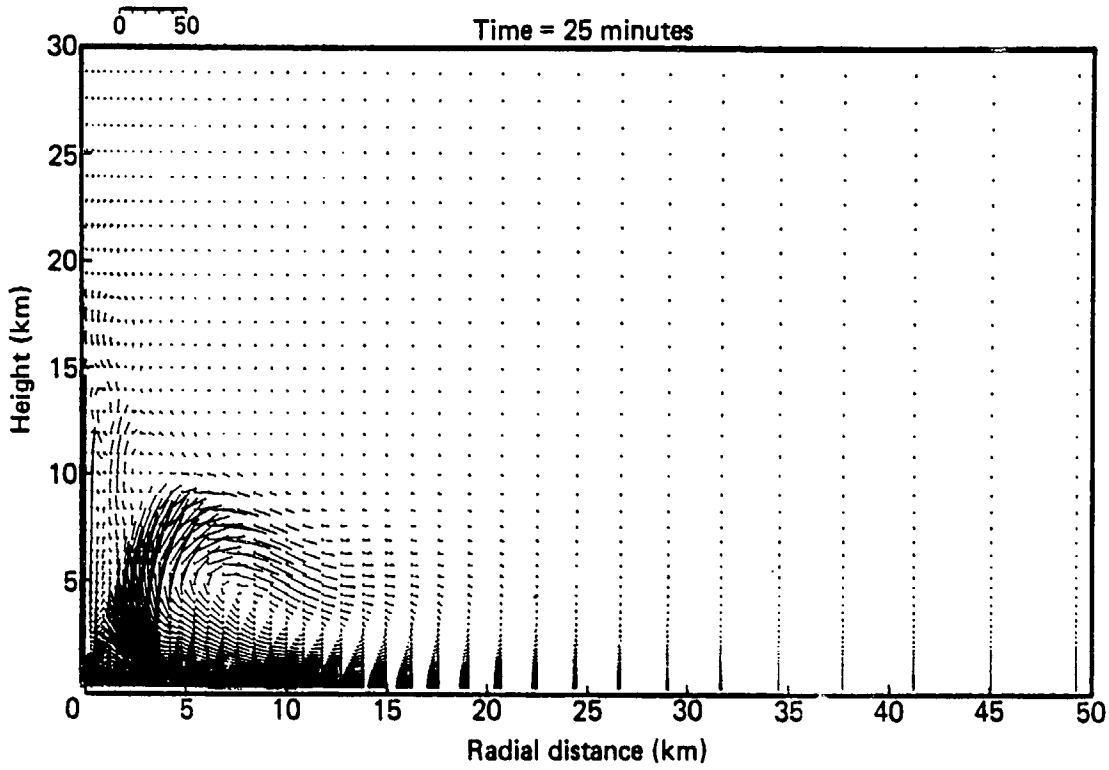

Figure 22. Velocity field generated by 10-km radius area fire at t = 25 min.

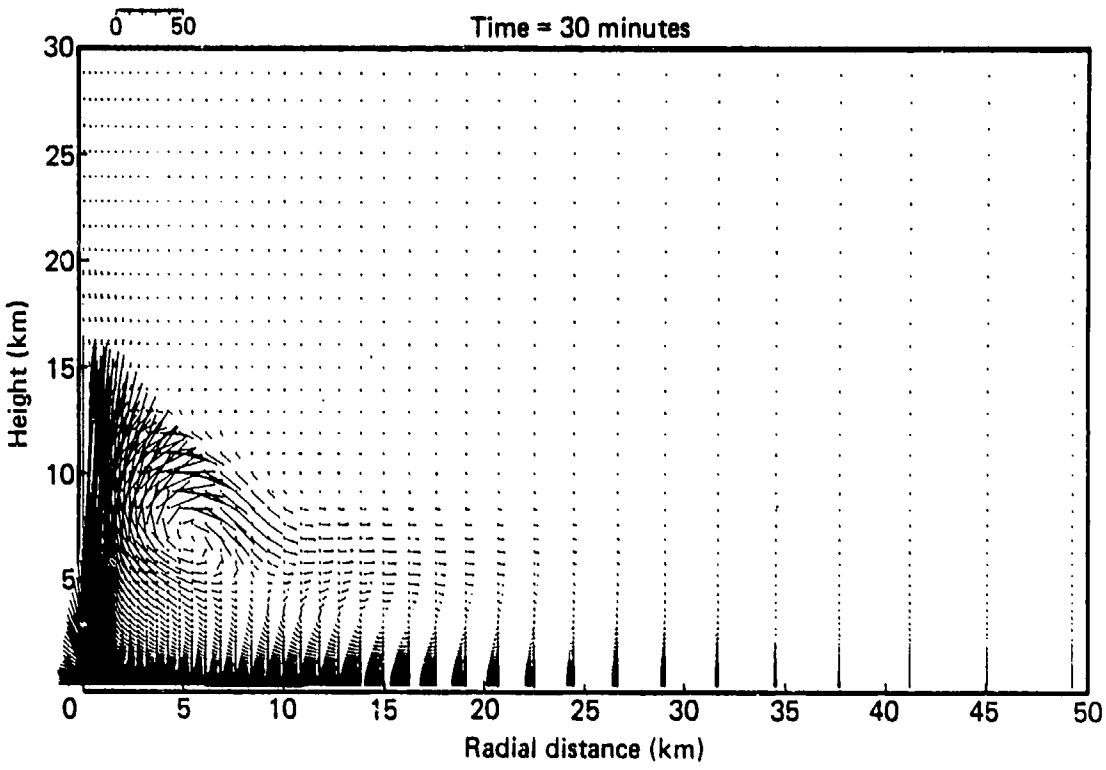

Figure 23. Velocity field generated by 10-km radius area fire at t = 30 min.

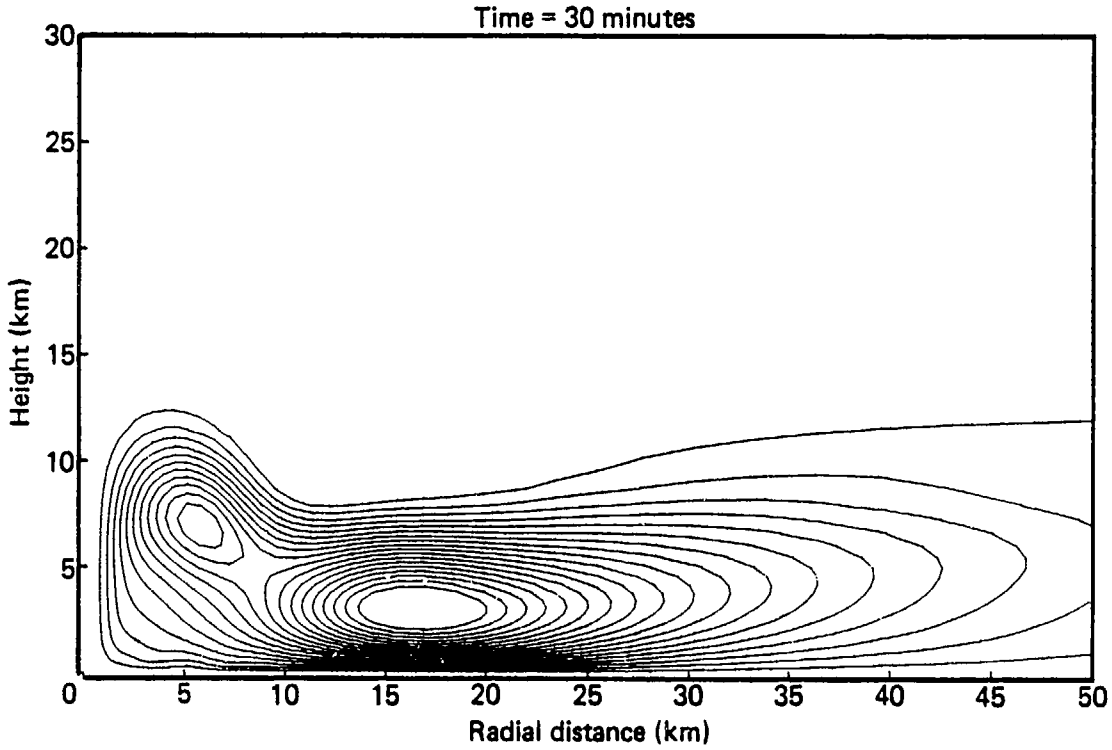

Figure 24. Streamlines generated by 10-km radius area fire at t = 30 min.

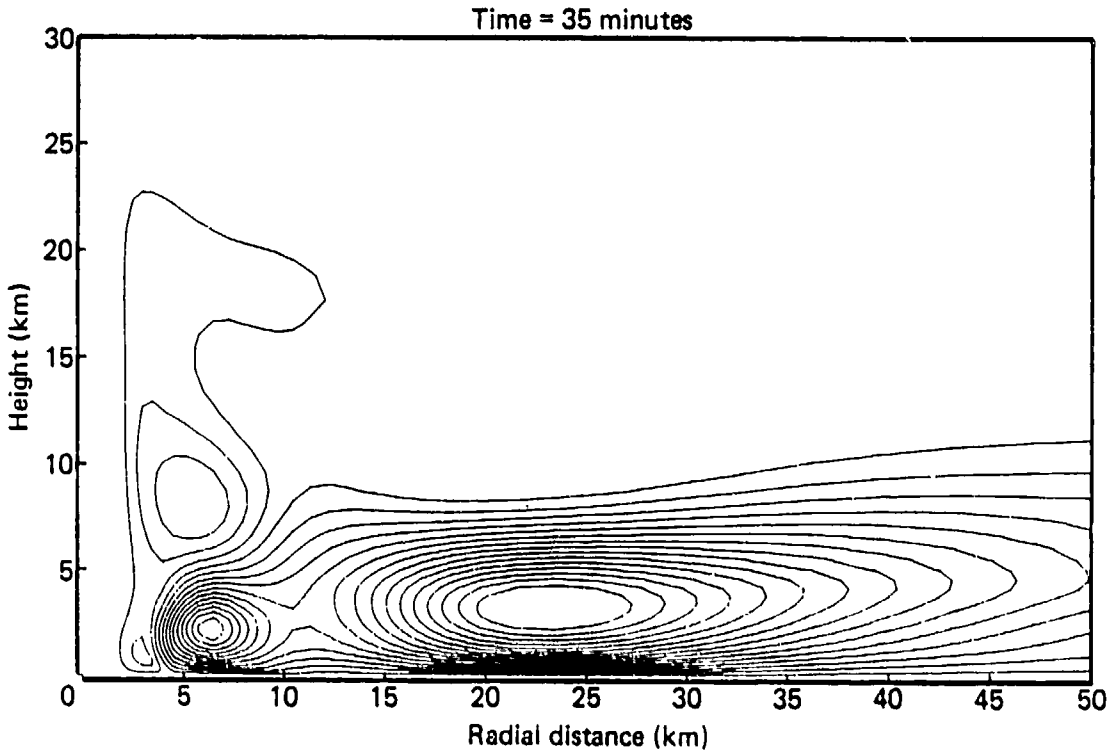

Figure 25. Streamlines generated by 10-km radius area fire at t = 35 min.

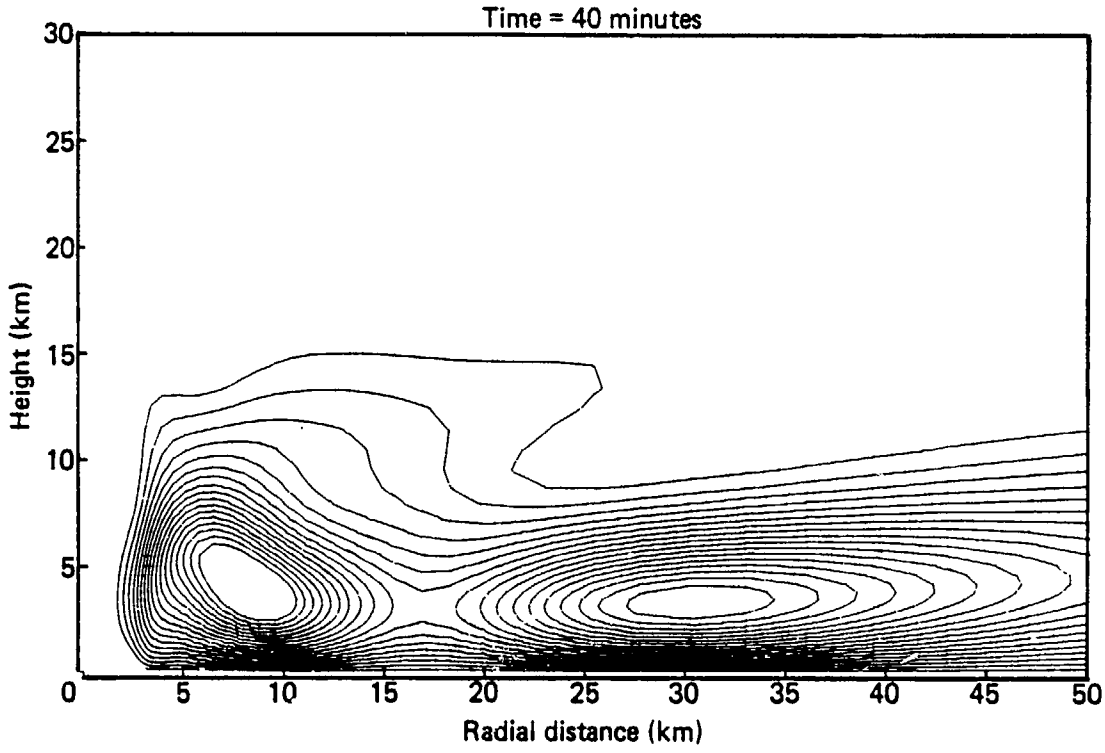

Figure 26. Streamlines generated by 10-km radius area fire at t = 40 min.

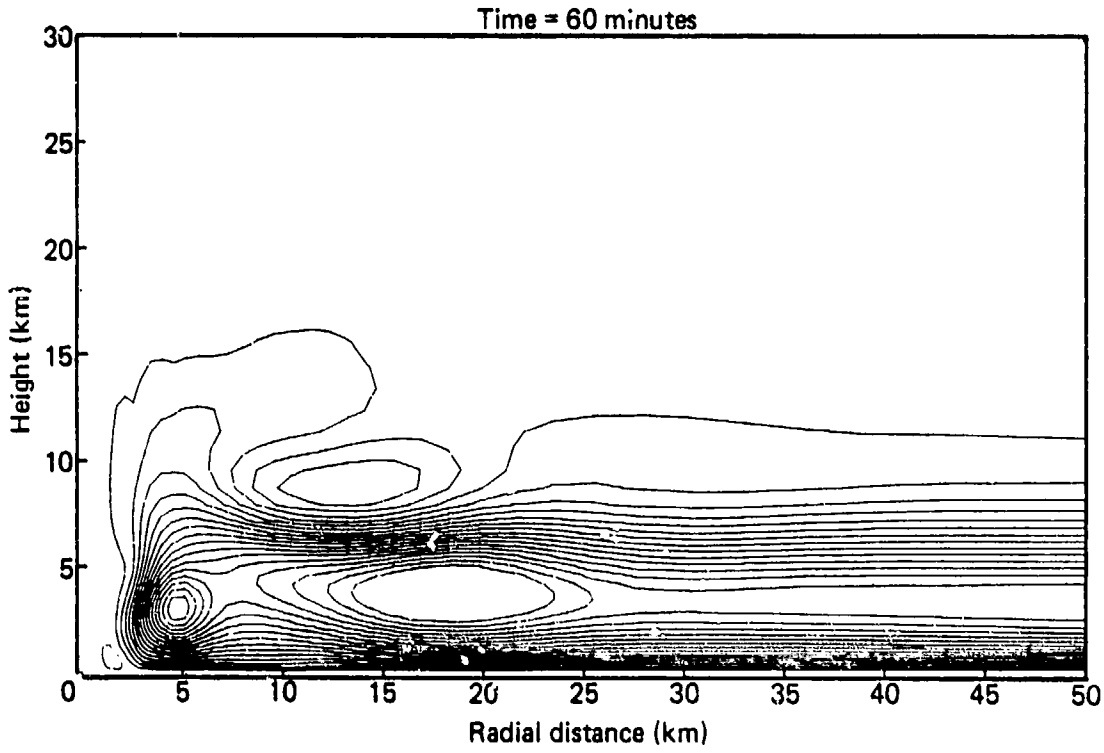

Figure 27. Streamlines generated by 10-km radius area fire at t = 60 min.

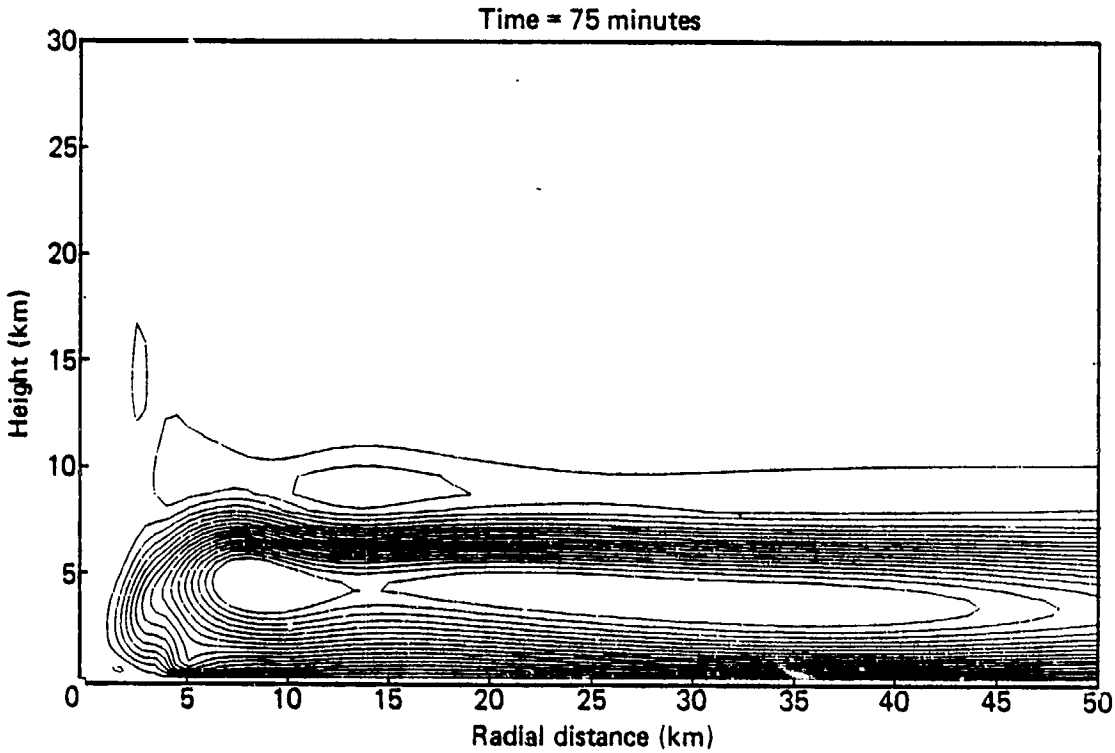

Figure 28. Streamlines generated by 10-km radius area fire at t = 75 min.

different times, these persistent vortices play a dominant role in the basic flow structure.

In general, the major mass transfers are contained by the atmosphere below the tropopause (11 km). Exceptions occur when periodic bursts, which we trace to the development of a series of corner centerline vortices, penetrate to higher altitudes. These motions are short-lived and appear to fall back to lower altitudes (cf. Figs. 25, 26, and 27). At approximately 60 min (Fig. 27), a counterclockwise vortex containing some of this material develops. At 75 min (Fig. 28), this vortex strengthens, superimposing a (particulate) layer upon the basic fire-plume flow.

In summary, a fairly complex flow is generated by a large area fire. Following a transient period characterized by a series of essentially local vortex motions, a strong buoyancy field is established that in turn leads to a persistent (40 to 50 m/s) radial inflow. This inflow of ambient air extends to approximately 45 km (the computation domain to 100 km), and is controlled in part by a strong vortex originally shed from the fire-plume periphery. The rising and turning of the convection plume are similarly influenced by vortices generated by the finite volume heat release. The major mass transfers are contained, by the atmosphere, in a clockwise rotation somewhat below the tropopause. At late times, however, a counter-rotating layer is formed above the primary flow, suggesting the development of distinct fire product strata.

The phenomena predicted both by the analytics and numerical simulation, although reasonable, require corroboration in some form. Scale experiments [Cermak, 1984] indicate that the basic flow features are indeed captured by the modeling. Another check is provided by a numerical simulation of Flambeau fire 460-7-66. Neither comparison is conclusive, but the results are encouraging.

The data specifications as well as documentation of the test results for fire 460-7-66 [Nielsen, 1970; Palmer, 1981] are more complete than those for other Flambeau fires. Nonetheless, there are a number of missing data; there is large experimental scatter in the results; and the documentation is incomplete. Despite these

shortcomings, we have numerically simulated this fire and have compared our results with those summarized by Nielsen [1970].

The two-dimensional SALE version was used in order to account for the ambient wind (2.2 m/s at ground level, rising to 10 m/s at 1900 m). The experimental fire consisted of 15 by 15 m fuel ricks separated by streets 7.5-m wide with total square cross sections of 330 m on a side. The grid resolves the heat region using 7.5 (x) by 3 m (y) zones near the ground. As a result, for the applied heat load, the time step is small and the calculation expensive. Accordingly, we have only carried the simulation to 8 min.

Figure 29 shows temperature profiles at 4 min. The heat addition peaks shortly thereafter and then decays rapidly. At 9.9 m the plume above each rick is still distinct. Somewhat above this height, the individual plumes begin to merge (note the smoothing of the temperature profiles in Fig. 29). The skewing of the upper plume is a result of the ambient wind tilting the plume.

Figures 30 through 32 show three views of the flow field. Due to the wind field, the flow is asymmetric, and similar to observation, the plume axis is moved in the windward direction. This is apparent in the early time (3 min) detail shown in Fig. 30. Ripples in the streamlines above the fire zone suggest an internal wave system set up by the fire.

Two rather strong vortex motions dominate the flow field even at early times. The lee-side vortex (around a bucyancy induced pressure deficit) appears to form as a result of the upwind fire-generated indraft at low level and plume outflow at higher levels. Similarly, the upstream vortex is a persistent feature of the flow. Initially, it forms near the fire and then rises with time. Both vortices stem from the strong enthalpy and entropy gradients (normal to the streamlines) established by the fire.

Figure 33 is a comparison of the results of our simulation (note that we use a westerly ambient wind rather than the actual southwesterly flow) with measurements reported by Nielsen [1970]. Although the comparison is quite good, we note a large spread in the test data (as well as some uncertainty in the test conditions), and thus must

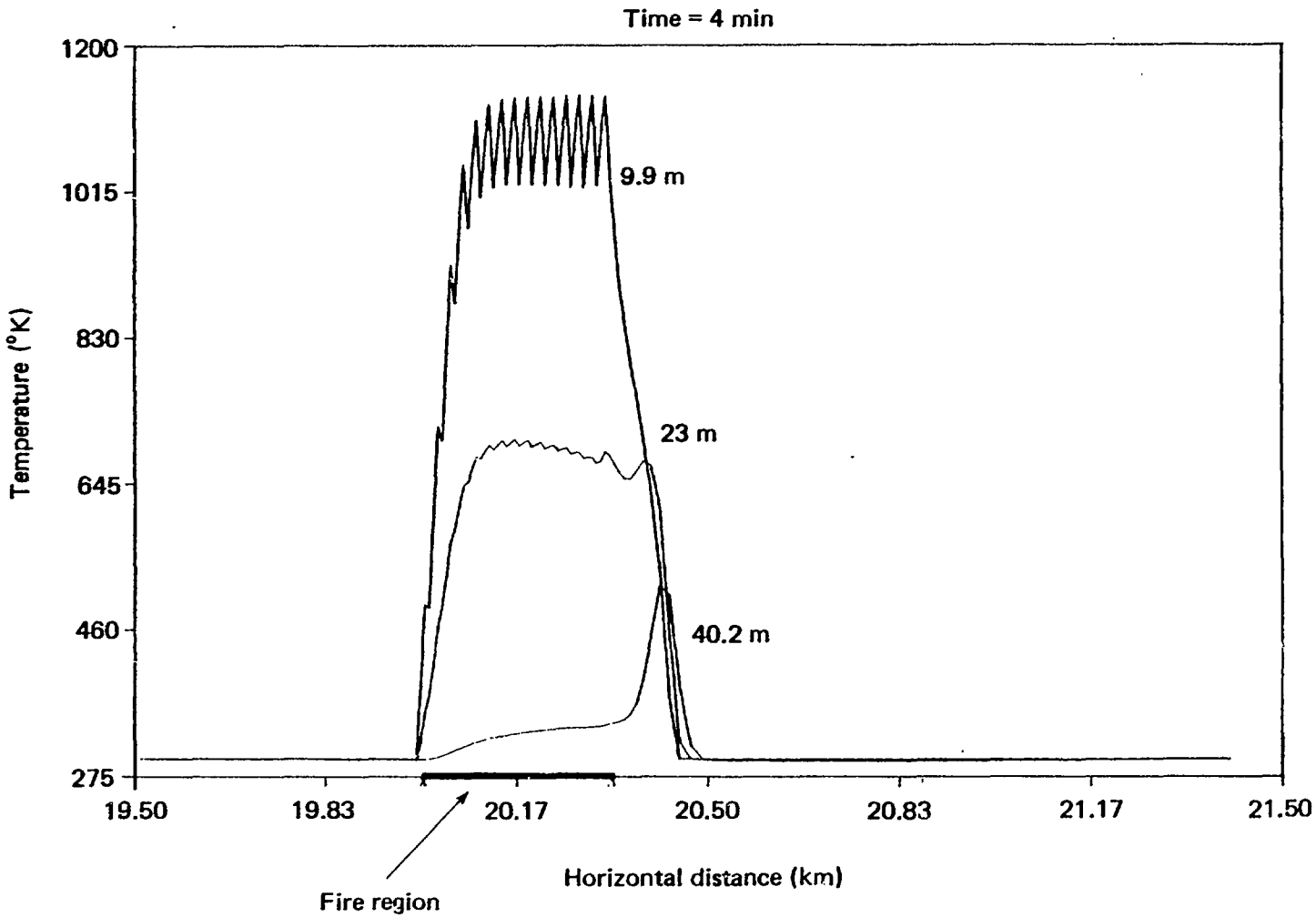

Figure 29. Temperature profiles above Flambeau fire 460-7-66 at t = 4 min.

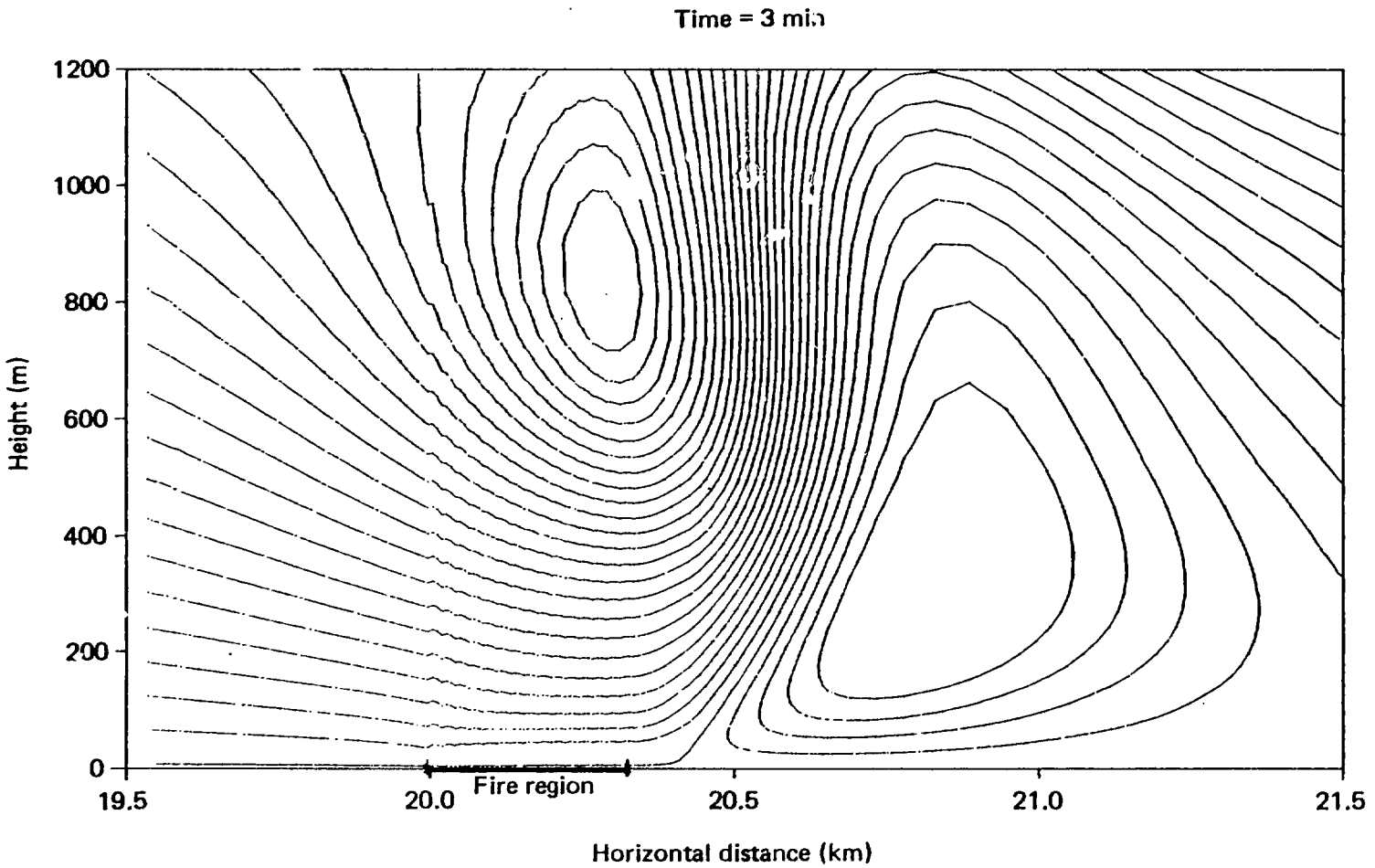

Figure 30. Streamlines showing early plume development above Flambeau fire 460-7-66 at t = 3 min.

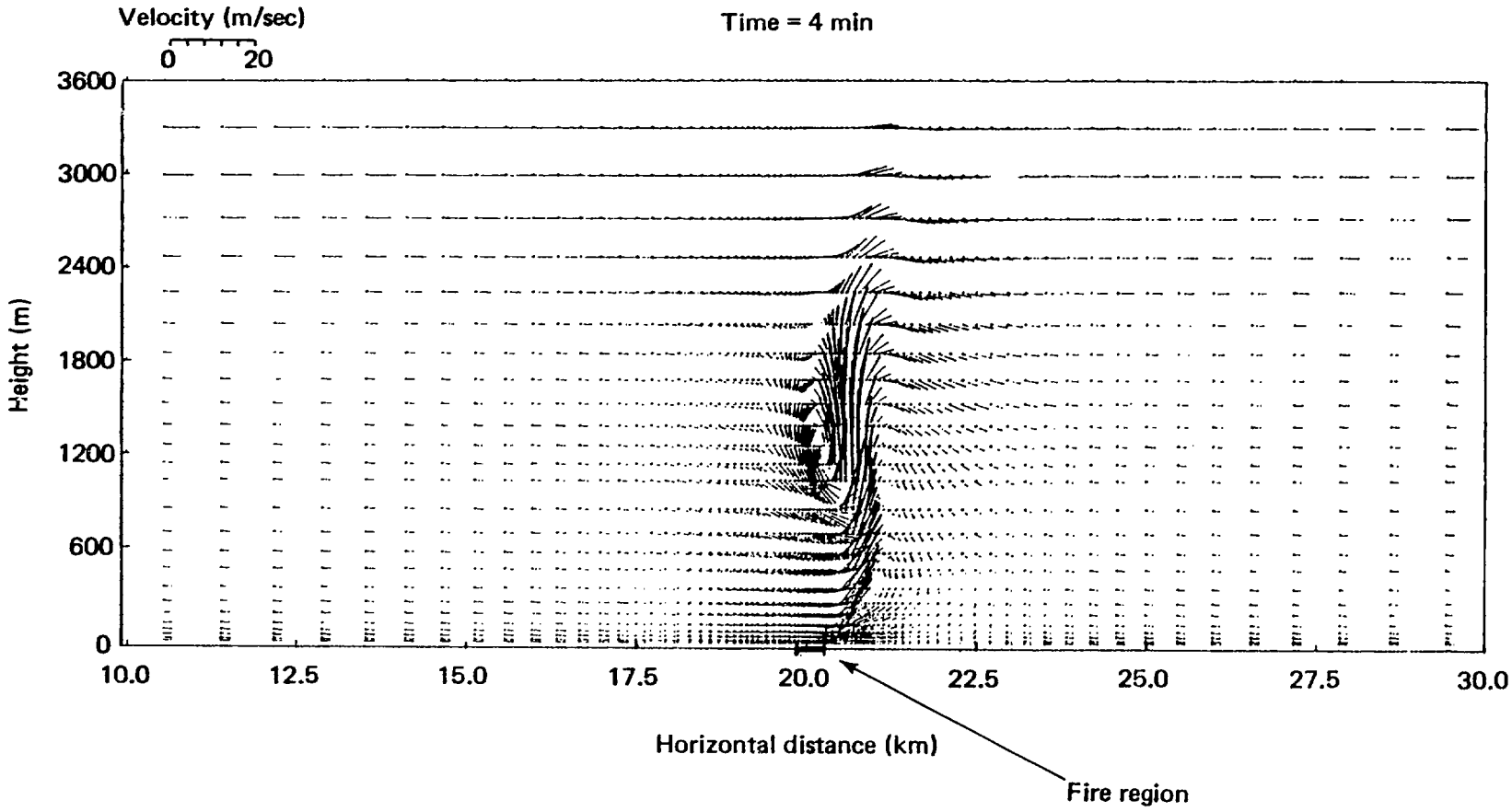

Figure 31. Vector plot showing plume rise above Flambeau fire 460-7-66 at t = 4 min.

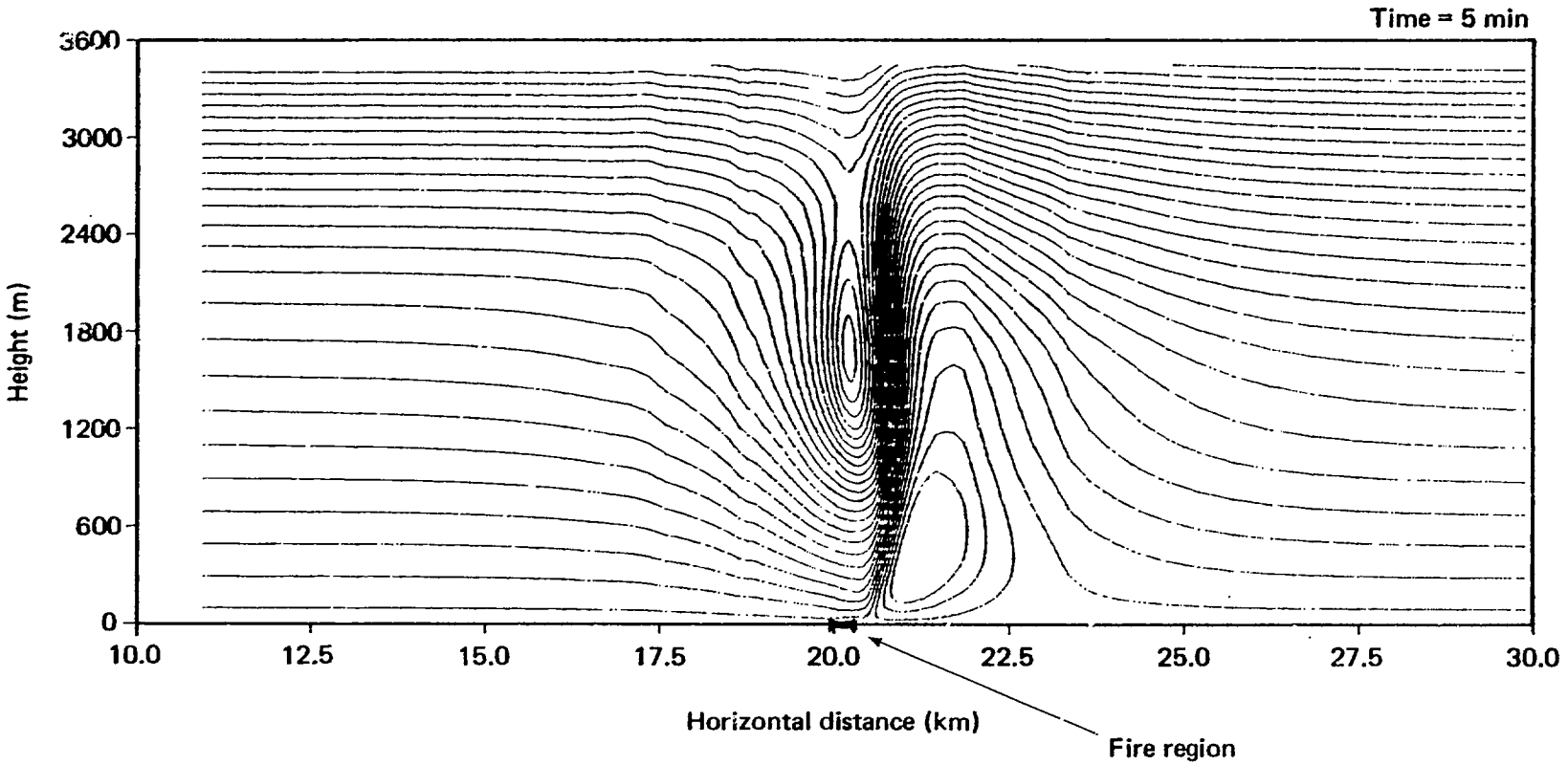

Figure 32. Streamlines generated by Flambeau fire 460-7-66 at t = 5 min.

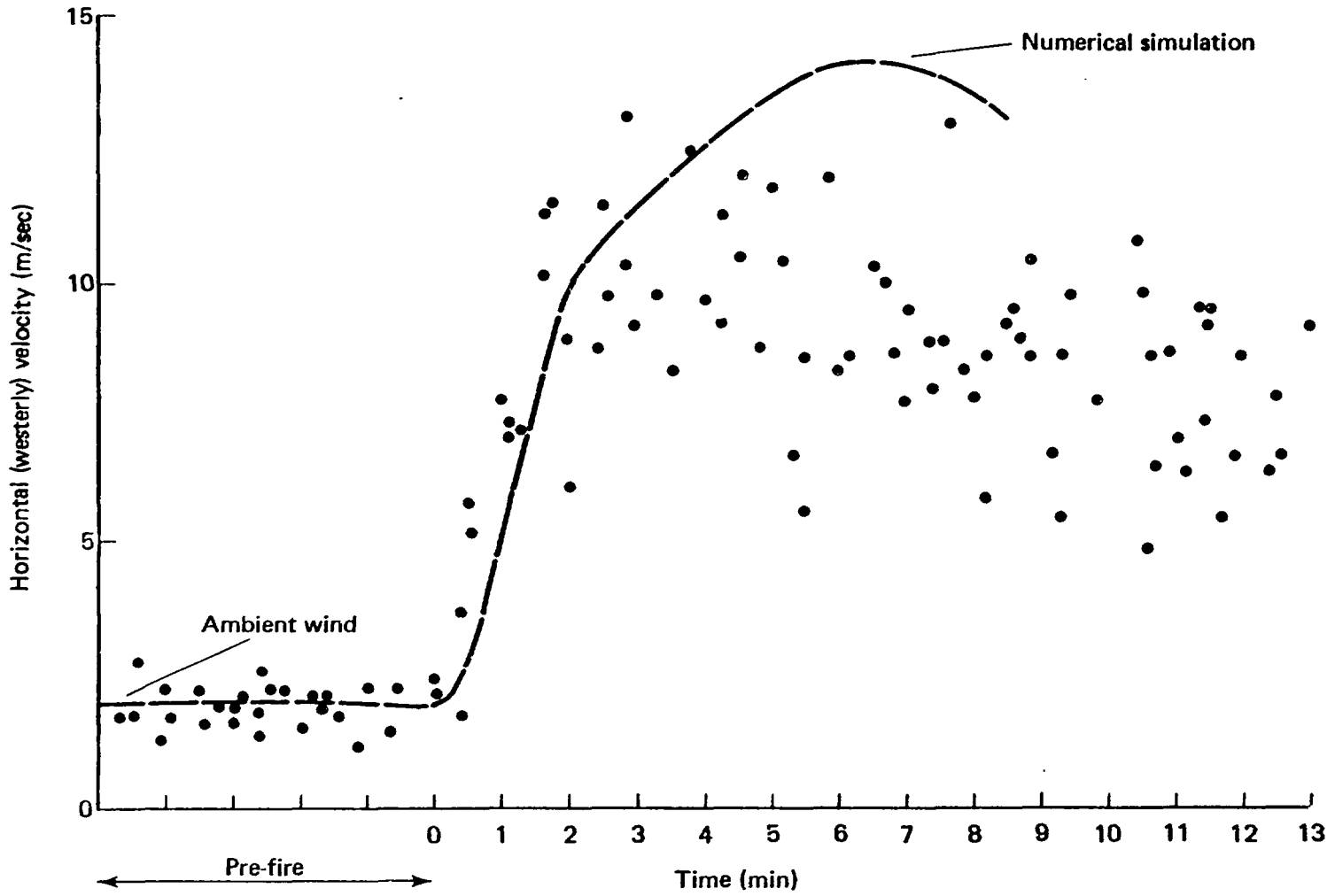

Figure 33. Comparison of calculated and measured velocities in Flambeau fire 460-7-66 at 8.25 m from west edge of fire and 6.3 m above ground.

temper any conclusions regarding model validity. Nevertheless, the main features of the complex flow of this field experiment have been simulated, with results that approximate reported observations.

The calculation reproduces plume rise that is limited by a moderate, ambient wind field, providing further evidence that the atmospheric state is a major factor in determining the ultimate disposition of combustion products.

DISCUSSION.

Both the quasi-steady analysis and the transient numerical results show the importance of the source region in predicting the atmospheric scale motions generated by a large fire. As a consequence, models are required for the combustion processes (heat release), radiative transfers, and turbulence. These interrelated processes control the flow evolution, and, in general, are not well modeled. Nevertheless, even simple models appear useful. The introduction of the fire energy within a finite volume seems superior to a prescribed surface thermal boundary condition.

There are, of course, other limitations. The air and combustion products are considered an ideal gas; particulates (smoke, ash, and brands) are neglected. Condensation is not considered in this study; the results are restricted to dry atmospheres. Including moisture can markedly affect plume dynamics and the resulting atmospheric response.

SECTION 3

LIST OF REFERENCES

Adams, J. S., D. W. Williams, and J. Tregellas-Williams, "Air Velocity, Temperature, and Radiant-Heat Measurements Within and Around a Large Free-Burning Fire," Fourteenth International Symposium on Combustion, The Combustion Institute, Pittsburgh, Pennsylvania, 1972, pp. 1045-1052.

Amsden, A. A., H. H. Ruppel, and C. W. Hirt, SALE: A Simplified ALE Computer Program for Fluid Flows at All Speeds, Los Alamos Scientific Laboratory, Los Alamos, New Mexico, 1980.

Carrier, G. F., F. E. Fendell, and P. S. Feldman, Firestorms, TRW Space and Technology Group, Redondo Beach, California, Document 38163-6001-UT-00, 1982.

Cermak, J., Colorado State University, Fort Collins, Colorado, private communication, November 15, 1984.

Countryman, C. M., Project Flambeau...An Investigation of Mass Fire (1964-1967), Vol. 1, U.S. Department of Agriculture, U.S. Forest Service, Berkeley, California, 1969.

Cox, G., and R. Chitty, "A Study of the Deterministic Properties of Unbounded Fire Plumes," Combust. Flame, Vol. 39, 1980, pp. 191-209.

Isaacson, E., and H. B. Keller, Analysis of Numerical Methods, John Wiley and Sons, New York City, 1966.

Larson, D. A., and R. D. Small, Analysis of the Large Urban Fire Environments, Pacific-Sierra Research Corporation, Report 1210, 1982.

Lommasson, T. E., R. K. Miller, R. G. Kirkpatrick, and J. A. Keller, A "Firestorm" Existence and Buildup Hypothesis, The Dikewood Corporation, Albuquerque, New Mexico, 1968.

Long, R. R., "Fire Storms," Fire Res. Abstr. Rev., 9, 1967, pp. 53-68.

Luti, F. H., "Some Characteristics of a Two-Dimensional Starting Mass Fire with Cross Flow," Comb. Sci. and Tech., Vol. 26, 1981, pp. 25-33.

Markatos, N. C., and G. Cox, "Hydrodynamics and Heat Transfer in Enclosures Containing a Fire Source," Physicochemical Hydrodynamics, Vol. 5, No. 1, 1984, pp. 53-66.

Markatos, N. C., M. R. Malin, and G. Cox, "Mathematical Modeling of Buoyancy Induced Smoke Flow in Enclosures," Int. J. Heat Mass Transfer, Vol. 25, 1982, pp. 63-75.

Markatos, N. C., and K. A. Pericleous, "An Investigation of Three-Dimensional Fires in Enclosures," Rev. Gen. Therm., Vol. 266, 1984, pp. 67-78.

McCaffrey, B. J., Purely Buoyant Diffusion Flames: Some Experimental Results, National Bureau of Standards, Washington, D.C., Report NBSIR79-1910, 1979.

Morton, B. R., G. I. Taylor, and J. S. Turner, "Turbulent Gravitational Convection from Maintained and Instantaneous Sources," Proc. R. Soc. London, Ser. A, Vol. 24, 1956, pp. 1-23.

Murgai, M. P., "Radiative Transfer Effects in Natural Convection Above Fires," J. Fluid. Mech., Vol. 12, 1962, pp. 441-448.

Nielsen, H. J., Mass Fire Data Analysis, IIT Research Institute, Chicago, Illinois, DASA Report 2018, 1970.

Palmer, T. Y., "Large Fire Winds, Gases, and Smoke," Atmos. Environ., Vol. 15, 1981, pp. 2079-2090.

Rosenblatt, M., Comparisons of Mass Fire Environments Involving a Factor of 4 Variations of Burning Rates for a 10 KM Radius Fire, California Research and Technology Inc., Chatsworth, California, 1983.

Small, R. D., and D. A. Larson, "Velocity Fields Generated by Large Fires," 26th Israel Annual Conference, Haifa, Israel, 1984, pp. 128-139.

Small, R. D., D. A. Larson, and H. L. Brode, Analysis of Large Urban Fires, Pacific-Sierra Research Corporation, Report 1122, 1981.

-----, "Asymptotically Large Area Fires," J. Heat Trans., Vol. 106, 1984, pp. 318-324.

Smith, R. K., "Radiation Effects on Large Fire Plumes," Eleventh International Symposium on Combustion, The Combustion Institute, Pittsburgh, Pennsylvania, 1967, pp. 507-515.

Smith, R. K., B. R. Morton, and L. M. Leslie, "The Role of Dynamic Pressure in Generating Fire Winds," J. Fluid, Mech., Vol. 68, 1975, pp. 1-19.

Thomas, P. H., "The Size of Flames from Natural Fires," Ninth International Symposium on Combustion, The Combustion Institute, Pittsburgh, Pennsylvania, 1963, pp. 844-859.

U. S. Forest Service, untitled films, Fire Laboratory, Riverside, California, 1967.

Zukoski, E. E., T. Kubota, and B. Cetegen, Entrainment in the Near Field of a Fire Plume, National Bureau of Standards, Washington, D.C., NBS-GCR-81-346, 1981.

DISTRIBUTION LIST

DEPARTMENT OF DEFENSE

DEFENSE INTELLIGENCE AGENCY
ATTN: DB-6E2 C WIEHLE
ATTN: RTS-2B
ATTN: WDB-4CR

DEFENSE NUCLEAR AGENCY
ATTN: OPNS
ATTN: RAAE
ATTN: RARP
ATTN: TDTD
4 CYS ATTN: TITL

DEFENSE TECHNICAL INFORMATION CENTER
12 CYS ATTN: DD

FIELD COMMAND DEFENSE NUCLEAR AGENCY
ATTN: FCTT W SUMMA
ATTN: FCTXE

JOINT STRAT TGT PLANNING STAFF
ATTN: JKCS

DEPARTMENT OF ENERGY

LAWRENCE LIVERMORE NATIONAL LAB
ATTN: J PENNER
ATTN: L-442, J BACKOVSKY
ATTN: N ALVAREZ
ATTN: R PERRETT

LOS ALAMOS NATIONAL LABORATORY
ATTN: DR D CAGLIOSTRO
ATTN: R MALONE

OTHER GOVERNMENT

DEPARTMENT OF COMMERCE
ATTN: H BAUM
ATTN: R LEVINE

DIRECTOR, FFASR
ATTN: C CHANDLER

FEDERAL EMERGENCYS MANAGEMENT AGENCY
ATTN: H TOVEY
ATTN: OFC OF RSCH/NP H TOVEY

NASA
ATTN: O TOON

NATIONAL CENTER ATMOSPHERIC RESEARCH
ATTN: S SCHNEIDER

DEPARTMENT OF DEFENSE CONTRACTORS

ASTER, INC
ATTN: G TRIPOLI

CALIFORNIA RESEARCH & TECHNOLOGY, INC
ATTN: M ROSENBLATT

CARPENTER RESEARCH CORP
ATTN: H J CARPENTER

CHARLES SCAWTHORN
ATTN: C SCAWTHORN

FACTORY MUTUAL RESEARCH CORP
ATTN: R FRIEDMAN

IIT RESEARCH INSTITUTE
ATTN: H NAPADENSKY

INSTITUTE FOR DEFENSE ANALYSES
ATTN: L SCHMIDT

KAMAN SCIENCES CORP
ATTN: E CONRAD

KAMAN TEMPO
ATTN: DASIAC

KAMAN TEMPO
ATTN: DASIAC

MISSION RESEARCH CORP
ATTN: J BALL

MODELING SYSTEM, INC
ATTN: G BERLIN

NOTRE DAME DU LAC, UNIV OF
ATTN: T J MASON

PACIFIC-SIERRA RESEARCH CORP
ATTN: H BRODE, CHAIRMAN SAGE
4 CYS ATTN: R SMALL
2 CYS ATTN: D LARSON
2 CYS ATTN: D REMETCH

R & D ASSOCIATES
ATTN: D HOLLIDAY
ATTN: F GILMORE
ATTN: R TURCO

RAND CORP
ATTN: P DAVIS

RAND CORP
ATTN: B BENNETT

SCIENCE APPLICATIONS INTL CORP
ATTN: M DRAKE
ATTN: M MCKAY

SCIENCE APPLICATIONS INTL CORP
ATTN: D BACON
ATTN: J COCKAYNE

SCIENTIFIC SERVICES, INC
ATTN: C WILTON

SRI INTERNATIONAL
ATTN: G ABRAHAMSON

STAN MARTIN ASSOCIATES
ATTN: S MARTIN

SWETL, INC
ATTN: T PALMER

TRW ELECTRONICS & DEFENSE SECTOR
ATTN: F FENDELL